A NONLOCAL KINETIC MODEL FOR PREDATOR-PREY INTERACTIONS IN TWO DIMENSIONS

by

Justin Meskas

B.Sc. (Mathematical Physics), Simon Fraser University, 2010

THESIS SUBMITTED IN PARTIAL FULFILLMENT

OF THE REQUIREMENTS FOR THE DEGREE OF

MASTER OF SCIENCE

IN THE

DEPARTMENT OF MATHEMATICS

FACULTY OF SCIENCE

SIMON FRASER UNIVERSITY

Summer 2012

APPROVAL

Name: Justin Meskas

Degree: Master of Science

Title of Thesis: A nonlocal kinetic model for predator-prey interactions in two dimensions

Examining Committee: Dr. David Muraki, Professor (Chair)

Dr. Razvan Fetecau
Senior Supervisor
Associate Professor

Dr. John Stockie
Supervisor
Associate Professor

Dr. JF Williams
Examiner
Associate Professor

Date Approved: August 7, 2012

Partial Copyright Licence

Abstract

Eulerian models based on integro-differential equations may be used to model collective behaviour, by treating the group of individuals as a population density. In comparison with Lagrangian models, where one tracks distinct individuals, Eulerian models are formulated as evolution equations for the density field, and hence permit rigorous analysis to be performed. The population densities are influenced by the social interactions of attraction, repulsion and alignment. We introduce a new model for predator-prey dynamics that generalizes a previous integro-differential equation model by introducing the predator dynamics and a blind zone for the prey. Extensive simulations were performed to showcase the realism of the model, and these simulations are presented in four stages. First, the prey reacts solely due to interactions with itself. Second, a stationary predator distribution is introduced. Third, the predator's distribution remains fixed but moves in a predetermined fashion. Finally, the predator dynamics are governed by equations analogous to those of the prey. Variations in the size of the blind zone for the prey are explored that can determine whether a prey cluster stays together or splits apart. The prey and predator demonstrate realistic behaviours that are seen in nature.

To my girlfriend, Sarah, for supporting me throughout all aspects of life.
And to my father, mother and sister for always let me follow my dreams,
even though they never knew what I was doing.

Acknowledgments

I would like to acknowledge and thank my supervisors Dr. Razvan Fetecau and Dr. John Stockie for all their advice, guidance and support.

Contents

List of Figures

Chapter 1

Introduction

In recent years many mathematical models have been introduced in an attempt to describe collective behaviour in animal groups. Seeing a biological aggregation, such as a flock of birds, one can easily become transfixed by the complexity of the movement of the group. Other forms of biological aggregations are a school of fish, a swarm of insects, or a herd of quadrupeds, as seen in Figure 1.1. Specific examples that are well known are: swarms of mosquitoes, bees or locusts; herds of caribou or zebra; a pod of orcas or a crowd of humans. A more complex system would be that of multiple types of groups such as a predator-prey relationship or two species competing for food. Some examples of multiple group behaviours are dolphins confining fish into a bait ball to make capture easier [33], wolves chasing white-tailed deer [34] and Eleonora's falcons' high diving speed technique to capture a bird in a flock[18].

The grouping behaviour of animals has advantages and disadvantages. One advantage is protection of which there are many forms. An animal in a group when in the presence of a predator will have a higher chance of survival than a solitary individual because there are more potential prey for the predator to catch. Also, if animals stay in groups, the chance that a roaming predator will find the group is less than that of finding scattered prey within a given space because the group occupies a smaller space than scattered individuals. Additionally, a school of fish can confuse a predator by appearing large and making it difficult for the predator to focus on only one fish [33]. Another example of protection is that the larger a school of fish is, the more predators are required to constrict the fish into a bait ball for easier capture [33]. One disadvantage of being in a group is

Figure 1.1: Animal groups: Some examples of collective behaviour. The top left image shows a school of fish. The top right image shows a flock of birds. The bottom left image shows a swarm of insects. The bottom right image shows a herd of ungulates. All images are from http://www.inspiremonkey.com/2010/08/20-magnificent-photographs-of-swarming-and-group-animals.

there may not be enough food for everyone when the group is foraging. Another disadvantage is an increase of predation because a large group is hard to hide. Despite the fact that finding a group takes a predator more time, a large group is still more conspicuous than an individual.

When models are created for biological aggregations they are commonly based on three social behavioural assumptions. These three assumptions are attraction, repulsion and alignment with neighbours. An individual in a group will be attracted to neighbours that are far away, repelled by neighbours that are too close, and align with neighbours that are neither too close nor too far away. Three concentric circles depict the zone of influence for each social interaction. The repulsion zone is centred in the middle with the alignment zone surrounding it. The attraction zone surrounds both repulsion and alignment zones. These three assumptions provide the foundation for most model types created to depict animal grouping.

There are two common types of models that are used to describe animal groups. The first is Lagrangian models which are particle based models that consist of discrete animals interacting with a finite number of neighbours. The second is Eulerian models which are partial differential equations or integro differential equations that describe the evolution of the population density field. The Lagrangian approach is a simple formulation of how each group member interacts with other nearby members [9]. This formulation shows, to reasonable precision, many real biological aggregations. However, it does not allow for rigorous analysis and becomes computationally expensive for a large number of individuals. The Eulerian approach, which can be classified as a continuum or kinetic version, commonly consists of a continuous population density that is convoluted with different social interaction kernels.

The approach in our research is to use a two dimensional, nonlocal kinetic partial differential equation model. The nonlocal nature of the model allows for both neighbours nearby and further away to also have an influence [12, 21, 31]. The kinetic aspect of the model allows for parallels to be made between biological aggregations and the more understood kinetic theory of gases [7]. Our research is a continuation of the work done by Fetecau in [13]. Fetecau extended the one dimensional model from [11] to a two dimensional model, which incorporated a formulation of angular orientation similar to [10, 14] to add the alignment interaction for the second dimension. Our research builds on the model in [13] by adding a blind zone and a predator. The blind zone produces a more realistic reaction behaviour of individuals since they cannot see behind themselves. Blind zones are commonly included in models of biological aggregations, such as in [9]. The addition of

a predator gives another layer of complexity because biological aggregates do not live in isolation from other species and are subject to predation.

There are many predator-prey models that are coupled difference or differential equations such as in [4, 19, 22]. These are popular because they give an overall idea of what the population size is and how the predator-prey relationship affects the population sizes. These models, however, do not address the local, small time scale behaviour of the predator-prey relationship such as predators' hunting strategies or prey avoidance strategies. In [2], a system of hyperbolic reaction-diffusion equations is used to describe the spatial-temporal dynamics of the predator-prey interactions. Since birth and death are incorporated, it emphasizes population fluctuations over a life cycle time scale. In [32], a cellular automata method is used to describe and predict the schooling behaviour of fish. In [16], Handegard et al. used sonar imaging to capture the behaviour of predator-prey dynamics. These last two predator-prey models are individual based models and our research uses the Eulerian approach to discover small time scale kinematics in predator-prey relationships, on which very little work has been done. Our model generates realistic qualitative results that can be related to specific examples of animal behaviour in nature.

Understanding animal group behaviour has important applications for various industries. For example the fishing industry would be able to apply more efficient capture techniques from knowing more about fish behaviour [24]. By applying similar animal movement models in robotics, robots are able to maintain a formation and perform navigational tasks and avoid hazards [1]. Similarly, this work has connections with military scouting of landscapes where a formation of autonomous vehicles direct their sensors to optimally scan a location[1, 8].

Chapter 2 discusses the model, which follows from the model in [13] and adds a blind zone and a predator. In Chapter 3 the numerical method is described. Chapter 4 shows many different animal behaviours that are captured with our model. These animal behaviours are split into four sections depending on the sophistication of the predator: no predator, stationary predator, a moving predator that does not respond to its surroundings, and a predator that turns and chases the prey depending on its surroundings.

Chapter 2

Model

The model is governed by the following integro-differential equation

$$\partial_t u + \gamma \vec{e}_\phi \cdot \nabla_{\vec{x}} u = -\lambda(\vec{x}, \phi)u + \int_{-\pi}^{\pi} T(\vec{x}, \phi', \phi)u(\vec{x}, \phi', t)d\phi', \tag{2.1}$$

where $u(\vec{x}, \phi, t)$ is the population density of individuals at spatial location $\vec{x}$ = (x, y), at time t and orientated in direction $\phi \in (-\pi, \pi]$, measured from the positive x-axis. The individuals are moving in the direction $\vec{e}_\phi = (\cos\phi, \sin\phi)$ with speed γ, which is a constant. The turning of individuals is modeled by $\lambda(\vec{x}, \phi)$ and $T(\vec{x}, \phi', \phi)$. These two functions model the turning rates of individuals and are dependent on the individuals' attraction, repulsion and alignment with each other. They will come together if the attraction factor is strong enough. The repulsion effect will cause two individuals to separate from each other, provided they are close enough. The alignment factor will cause individuals to change direction to align with their neighbours. The implementation of these three factors will be discussed in Section 2.1. The turning rate $\lambda(\vec{x}, \phi)$ is the rate at which the individuals in the state $(\vec{x}, \phi)$ will want to turn. The larger the λ, the more likely the individual will turn. $T(\vec{x}, \phi', \phi)$ describes how individuals located at $\vec{x}$ will reorient themselves from ϕ' to ϕ. The model depicts an individual's decision to continue in its current direction or to turn based on its neighbours. We assume that the only two factors that influence turning are the distance from neighbours and the neighbours' orientation. The three rules of attraction, repulsion and alignment are contained in these two factors.

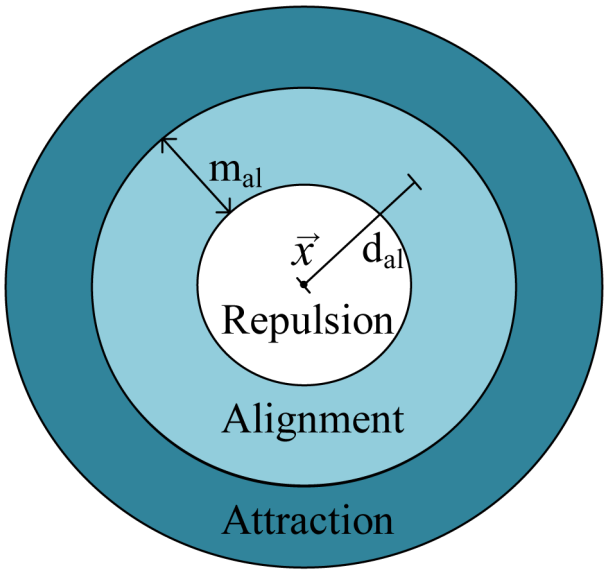

Figure 2.1: Zones of repulsion, alignment and attraction: The decision making individual is located at $\vec{x}$ and can turn away from neighbours in the repulsion zone, turn to align with neighbours in the alignment zone or turn to approach neighbours in the attraction zone. The radius and width of each zone is determined by d_j and m_j, respectively, where j = a, r, al.

2.1 Factors of Influence

Every individual is influenced by every other individual's position and direction. The position, but not the direction, of the other individuals is embedded into three distance kernels. However, the position and the direction of the other individuals are embedded in three orientation kernels. In each case the three types are attraction, repulsion and alignment, which makes for six kernels.

- 19 Distance Kernels:

  Each distance kernel, K_j^d, is represented by a zone which is centred on the decision making individual, $\vec{x}$; with variations of the radius, d_j, of the zones; and variations of the width, m_j, of the zones (see Figure 2.1); and is defined by

  $$K_j^d(\vec{x}) = \frac{1}{A_j} e^{-\left(\sqrt{x^2+y^2}-d_j\right)^2/m_j^2}, j = a, r, al. \tag{2.2}$$

  There are three kernels, which may overlap, one for each j ($j = a$ for attraction, $j = r$ for repulsion, and $j = al$ for alignment). The A_j's are renormalizing constants that force the

spatial integral of the kernel to equal 1. It can be shown that these constants are

$$A_j = \pi m_j \left(m_j e^{-d_j^2/m_j^2} + \sqrt{\pi} d_j \left(1 + \operatorname{erf}\left(d_j/m_j\right)\right)\right). \tag{2.3}$$

- Orientation Kernels:

  The attraction kernel, K_a^o, is

$$K_a^o\left(\vec{s};\vec{x},\phi\right) = \frac{1}{2\pi}\left(-\cos\left(\phi-\psi\right)+1\right). \tag{2.4}$$

  The direction the decision making individual is heading is ϕ, while ψ is the direction to another individual from the decision making individual, as seen in Figure 2.2. K_a^o is smallest when ϕ and ψ are the same. This will happen when the decision making individual is directed towards its neighbour. K_a^o is largest when ϕ and ψ are an angle of π away from each other. If the neighbouring individual is directly behind the decision making individual, there is a higher likelihood of the decision making individual turning to approach its neighbour. This means that the decision making individual at $\vec{x}$ in Figure 2.2 is more likely to turn because of the attractive influences of $\vec{s'}$ compared to $\vec{s}$. The $\frac{1}{2\pi}$ factor renormalizes the kernel so it integrates to 1. Equation (2.4) suggests that K_a^o is a function of $\vec{s}$, $\vec{x}$ and ϕ. To show this we take the right hand side and expand the cosine with the trigonometric identity

$$\cos(\phi-\psi) = \cos\phi\cos\psi + \sin\phi\sin\psi, \tag{2.5}$$

  and we use

$$\cos\psi = \frac{s_x}{\sqrt{s_x^2+s_y^2}}, \qquad \sin\psi = \frac{s_y}{\sqrt{s_x^2+s_y^2}}, \tag{2.6}$$

  where s_x is the difference of the x coordinates of $\vec{x}$ and $\vec{s}$, and s_y is the difference of the y coordinates of $\vec{x}$ and $\vec{s}$. Putting this together gives

$$K_a^o\left(\vec{s};\vec{x},\phi\right) = \frac{1}{2\pi}\left(-\cos\phi\frac{s_x}{\sqrt{s_x^2+s_y^2}} - \sin\phi\frac{s_y}{\sqrt{s_x^2+s_y^2}} + 1\right). \tag{2.7}$$

  We do not know the ψ variable in Equation (2.4), the angle between individuals, ψ, however we know the variables in Equation (2.7), the location and direction of individuals, $\vec{x}$ and ϕ, respectively.

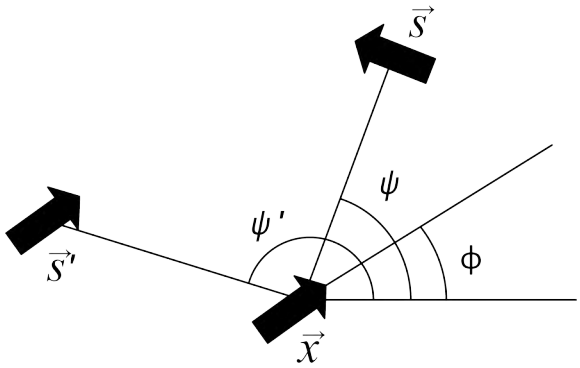

Figure 2.2: Orientation for attraction and repulsion: The decision making individual is located at $\vec{x}$ and is moving in direction ϕ. It is influenced to turn or not by the position of all its neighbours. Two such neighbours are located at $\vec{s}$ and $\vec{s'}$. The neighbour at $\vec{s'}$ influences the decision making individual to turn from attraction more than $\vec{s}$, while $\vec{s}$ influences the decision making individual to turn from repulsion more than $\vec{s'}$.

The repulsion kernel, K_r^o, is

$$K_r^o\left(\vec{s};\vec{x},\phi\right) = \frac{1}{2\pi}\left(\cos\left(\phi-\psi\right)+1\right). \tag{2.8}$$

This kernel is similar to the attraction kernel except there is no negative sign in front of the cosine term. The absence of the negative sign changes the behaviour of the decision making individual to be opposite from that of the attraction kernel. If the neighbour is in front of the individual, then the individual is more inclined to turn. If the neighbour is behind the individual, then the individual is more likely going to continue on its path. The decision making individual is more likely to turn in Figure 2.2 from influences from $\vec{s}$ compared to influences from $\vec{s'}$. Following a similar approach to Equations (2.5) - (2.7) we can write Equation (2.8) as

$$K_r^o\left(\vec{s};\vec{x},\phi\right) = \frac{1}{2\pi}\left(\cos\phi\frac{s_x}{\sqrt{s_x^2+s_y^2}}+\sin\phi\frac{s_y}{\sqrt{s_x^2+s_y^2}}+1\right). \tag{2.9}$$

Equation (2.9) is just a change of variable from Equation (2.8), which makes the kernel directly related to the known variables from each individual, its location,$\vec{x}$ and its direction, ϕ.

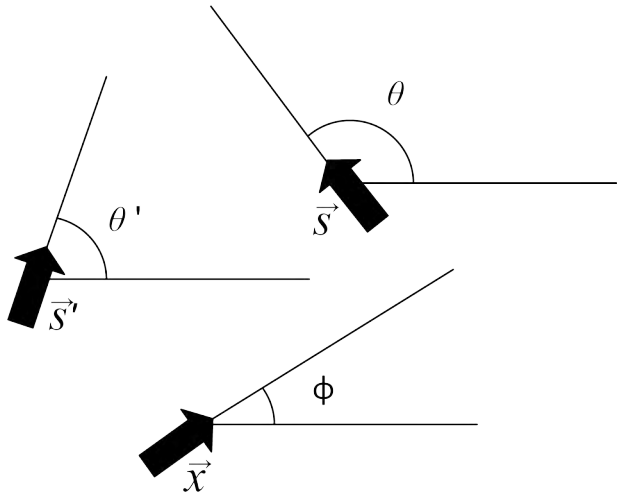

Figure 2.3: Orientation for alignment: The decision making individual located at $\vec{x}$ is influenced to turn to align with its neighbours. Two possible neighbours are $\vec{s}$ and $\vec{s'}$. The neighbour located at $\vec{s}$ moving in direction θ will influence the decision making individual more than $\vec{s'}$ because $|\theta - \phi|$ is larger than $|\theta' - \phi|$.

The alignment kernel, K^o_{al}, is different from the other two because it depends on the direction of the neighbours, not on their position, and is defined by

$$K^o_{al}(\theta, \phi) = \frac{1}{2\pi}\left(-\cos(\phi - \theta) + 1\right). \tag{2.10}$$

The direction the neighbour is moving is given by θ and is shown in Figure 2.3. K^o_{al} is smallest when the decision making individual is moving with the same angle as its neighbour ($\phi = \theta$). K^o_{al} is largest when they are orientated in opposite directions. The decision making individual will be influenced more by neighbour $\vec{s}$ in Figure 2.3 than neighbour $\vec{s'}$ because the direction the neighbour $\vec{s}$ is traveling is less aligned to the decision making individual's direction.

The six kernels from Equations (2.2), (2.7), (2.9) and (2.10) are the building blocks for both turning rate functions, λ and T. The development of these two functions is discussed in Sections 2.2 and 2.3.

2.2 Modeling the turning rate

The $\lambda(\vec{x}, \phi)$ in Equation (2.1) is be split into three terms according to the contributions from attraction, repulsion and alignment.

$$\lambda(\vec{x}, \phi) = \lambda_a(\vec{x}, \phi) + \lambda_r(\vec{x}, \phi) + \lambda_{al}(\vec{x}, \phi). \tag{2.11}$$

The attraction turning rate, λ_a, uses the two attraction kernels discussed in Section 2.1 and is described by the function

$$\lambda_a(\vec{x}, \phi) = q_a \int_{\mathbb{R}^2} \int_{-\pi}^{\pi} K_a^d(\vec{x} - \vec{s}) K_a^o(\vec{s}; \vec{x}, \phi) u(\vec{s}, \theta, t) d\theta d\vec{s}. \tag{2.12}$$

The attraction kernels, K_a^d and K_a^o, are dependent on $\vec{x} - \vec{s}$, which is the distance between two individuals located at $\vec{x}$, the decision making individual, and $\vec{s}$, the neighbour. The integral is over $\vec{s}$ and θ, which accounts for all neighbours' positions and directions, respectively. Since the kernels are both normalized, the size of λ_a is determined by a constant q_a, which is called the strength of attraction. Equation (2.12) can be visualized by taking all individuals separately in a two dimensional domain, and then weighting them according to both of the kernels, K_a^d and K_a^o. Areas that have a large weight in both the distance and orientation kernels as well as high population, u, will be the areas with large λ_a and hence a high likelihood of the decision making individual turning, as visualized in Figure 2.4. The two kernels shown in the first row of Figure 2.4 have the decision making individual centred at $\vec{x}$ = (0,0), with direction $\phi = 0$ facing the right. The population density u, shown in the bottom left of Figure 2.4 is integrated over all θ's. The figure for λ_a can be imagined by centering the two kernels at every spatial location on the plot of u, by calculating the rate of turning at every location with weight from the kernels and then by setting λ_a to the value at each location. Since λ_a is three dimensional the plot shown for λ_a is only for the individuals who are moving with angle $\phi = 0$. If a different direction is chosen for the decision making individual, the plots will be the same except it will be rotated to that particular direction.

The repulsion turning rate, λ_r, uses its two associated kernels, K_r^d and K_r^o, from Section 2.1 and is defined by

$$\lambda_r(\vec{x}, \phi) = q_r \int_{\mathbb{R}^2} \int_{-\pi}^{\pi} K_r^d(\vec{x} - \vec{s}) K_r^o(\vec{s}; \vec{x}.\phi) u(\vec{s}, \theta, t) d\theta d\vec{s}. \tag{2.13}$$

The repulsion kernels, K_r^d and K_r^o, depend on $\vec{x} - \vec{s}$. The size of λ_r is dependent on the strength

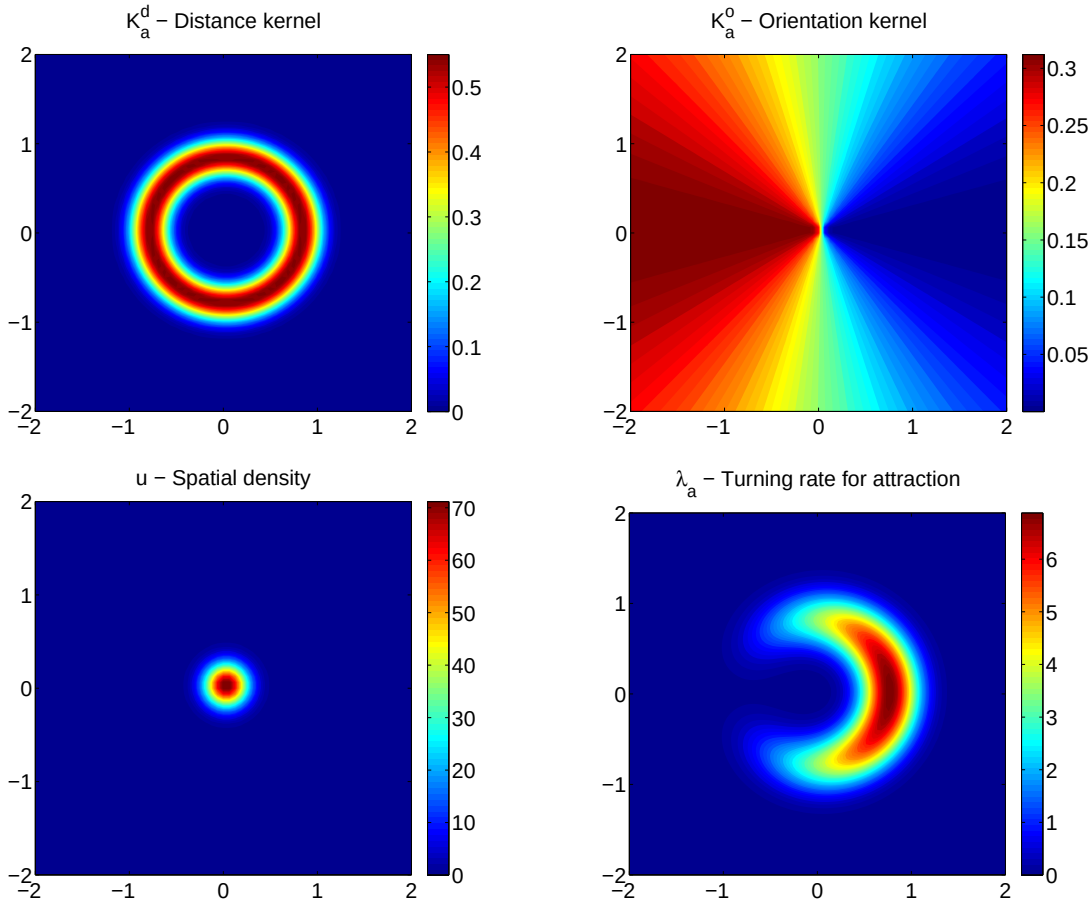

Figure 2.4: Building of λ_a: By picking a point in the population density plot (bottom left), and using the distance kernel plot (top left) and the orientation kernel plot (top right) centred at this point, the likelihood of the individual turning at this point can be calculated. This process can be repeated for all points in u. Since λ_a is three dimensional, all that can be shown here is the individuals moving to the right. The individuals in the high density regions of the λ_a plot (bottom right) are moving to the right and now will turn to approach individuals in the centre of the population density.

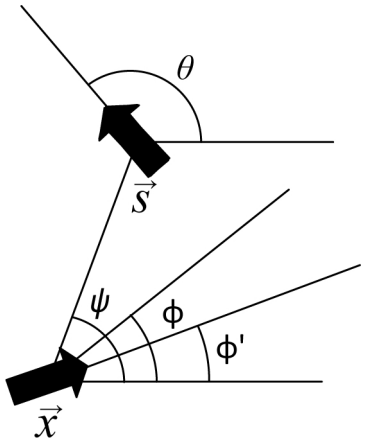

Figure 2.5: Orientation for T: The decision making individual at $\vec{x}$ moving with direction ϕ' has a probability of turning to direction ϕ based on all surrounding neighbours. One such neighbour is shown at location $\vec{s}$.

of repulsion, q_r. Areas with high density in K_r^d, K_r^o and u will cause a higher likelihood of the decision making individual to turn to avoid collision with its neighbours.

The alignment turning rate, λ_{al}, is different than the previous two and is defined by

$$\lambda_{al}(\vec{x},\phi) = q_{al}\int_{\mathbb{R}^2}\int_{-\pi}^{\pi} K_{al}^d(\vec{x}-\vec{s})K_{al}^o(\theta;\phi)u(\vec{s},\theta,t)d\theta d\vec{s}. \tag{2.14}$$

The alignment distance kernel, K_{al}^d, is still dependent on $\vec{x}-\vec{s}$, but now the orientation kernel, K_{al}^o, is dependent on θ. The direction the neighbours are moving, θ, influences the turning of the decision making individual. Areas with high density in K_{al}^d, K_{al}^o and u causes the decision making individual to turn to align with its neighbours.

2.3 Modeling the reorientation terms

The reorientation function $T(\vec{x},\phi',\phi)$ describes the rate at which an individual located at $\vec{x}$ will reorient itself from ϕ' to ϕ because of the influences of its neighbours (see Figure 2.5). The $T(\vec{x},\phi',\phi)$, in Equation (2.1), can be split into three terms according to the contributions from attraction, repulsion and alignment.

$$T(\vec{x},\phi',\phi) = T_a(\vec{x},\phi',\phi) + T_r(\vec{x},\phi',\phi) + T_{al}(\vec{x},\phi',\phi). \tag{2.15}$$

Looking at the contribution from attraction we have

$$T_a(\vec{x}, \phi', \phi) = q_a \int_{\mathbb{R}^2} \int_{-\pi}^{\pi} K_a^d(\vec{x} - \vec{s}) K_a^o(\vec{s}; \vec{x}, \phi') w_a(\phi' - \phi, \phi' - \psi) u(\vec{s}, \theta, t) d\theta d\vec{s}. \tag{2.16}$$

The same kernels for λ_a are also used here, as well as the constant q_a. Notice the variable in the K_a^o term describing the direction of the decision making individual has changed ϕ', instead of ϕ from Equation (2.12). This is done to eliminate the ϕ' variable in Equation (2.1) and to make the variables consistent after taking the integral. The major difference between the definitions of T_a and λ_a is the probability function w_a. The w_a gives the probability of turning from ϕ' to ϕ because of the interactions with neighbours located at $\vec{s}$. Each T_j has its respective $w_j (j = a, ral)$. Since w_a is a probability density function, we have

$$\int_{-\pi}^{\pi} w_a \left(\phi' - \phi, \phi' - \psi\right) d\phi = 1. \tag{2.17}$$

The probability density function w_a is described by

$$w_a \left(\phi' - \phi, \phi' - \psi\right) = g_{\sigma a} \left(\phi' - \phi - v_a \left(\phi' - \psi\right)\right), \tag{2.18}$$

where $g_{\sigma a}$ is an approximation of the delta function. In order to minimize confusion, the attraction subscript was chosen instead of a more general subscript. The decision making individual can turn toward any direction within a specific range. This range is centred around direction

$$\phi = \phi' - v_a \left(\phi' - \psi\right),$$

which is found by setting the argument of the function $g_{\sigma a}$ to zero. The parameter $\sigma > 0$ measures the width of the turning range the decision making individual will move into. The smaller the σ, the more accurate the turning. If σ is large, then the range is wide and the decision making individual can move anywhere within the range (See Figure 2.6).

The function to describe $g_{\sigma a}$ is

$$g_{\sigma a} \left(\eta_1\right) = \frac{1}{\sqrt{\pi}\sigma} \sum_{z \in \mathbb{Z}} e^{-\left(\frac{\eta_1 + 2\pi z}{\sigma}\right)^2}. \tag{2.19}$$

The function $g_{\sigma a}$ is a periodic Gaussian which obtains extra contributions from full rotations (see Figure 2.7). The rotations occur due to the integer nature of z, which is needed because the argument of $g_{\sigma a}$ could be as large as $2\pi + 1$. This amount is larger than 2π and we do not want individuals trying to rotate more than a full rotation. Therefore the integer nature of $g_{\sigma a}$ takes the contribution

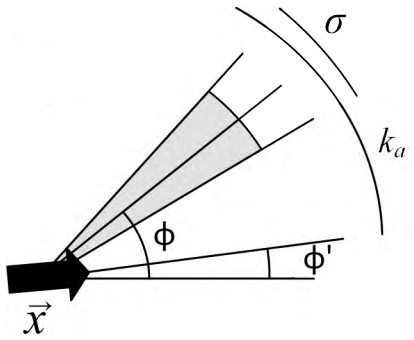

Figure 2.6: Visual aide for function g_σ: The decision making individual at $\vec{x}$ moving in direction ϕ' has a probability to turn to a direction near ϕ, with maximum turning possibility of k_a and with uncertainty related to σ.

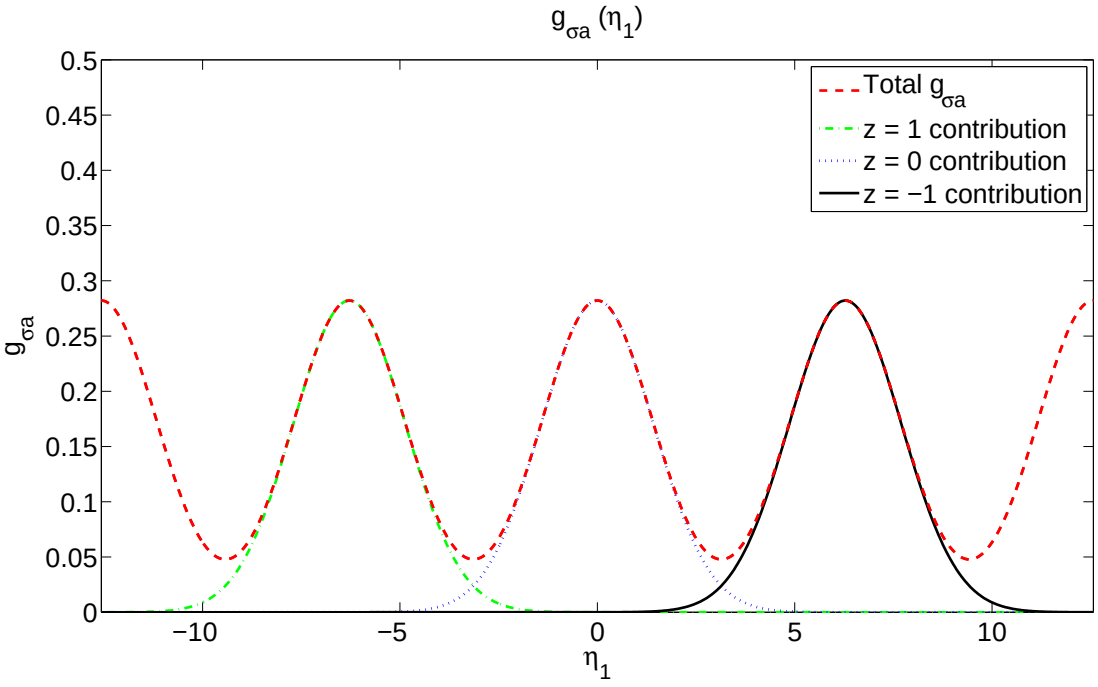

Figure 2.7: Function $g_{\sigma a}$: The red dashed curve shows the periodic Gaussian nature of the total $g_{\sigma a}$ function. The contributions from $z = 1$, 0, and -1 are shown by the green dash-dots, blue hash marks, and black solid curve, respectively. There are contributions from z as every integer, though not shown. To clearly illustrate the summation nature of $g_{\sigma a}$, a very large value of σ was chosen ($\sigma = 2$).

from the modulus of 2π of the argument. One can see from Equation (2.19) that if $-\pi < \eta_1 < \pi$ then the Gaussian giving the largest contribution is when $z = 0$. If $\pi < \eta_1 < 3\pi$ then the Gaussian giving the largest contribution is when $z = -1$. In fact, the contributions from a full rotation away are practically zero in comparison to the one giving the largest contribution.

The turning function, v_a, is defined as

$$v_a(\eta_2) = k_a \sin \eta_2. \tag{2.20}$$

k_a is a constant between 0 and 1, which gives the strength of attraction. Though this seems similar to q_a, they are different. While q_a describes the general strength of influence the neighbours have on the decision making individual, k_a describes how much the decision making individual will turn in certain directions. The decision making individual will turn at an angle relative to the size of k_a (see Figure 2.6).

Having a sine factor in the v_a function is not ideal. An alternative is $v_a(\eta_2) = k_a\eta_2$, which is more biologically realistic. If the decision making individual has another individual behind it then it should be influenced to turn more than if the neighbour was beside it. The v_a in Equation (2.20) has the maximum when the neighbours are beside, however this v_a is chosen because it is periodic and works well with the fast Fourier transform, which this model is based on and will be discussed further in Chapter 3.

T_r and T_{al} from Equation (2.15) are define by

$$T_r(\vec{x}, \phi', \phi) = q_r \int_{\mathbb{R}^2} \int_{-\pi}^{\pi} K_r^d(\vec{x} - \vec{s}) K_r^o(\vec{s}; \vec{x}, \phi') w_r(\phi' - \phi, \phi' - \psi) u(\vec{s}, \theta, t) d\theta d\vec{s}, \tag{2.21}$$

$$T_{al}(\vec{x}, \phi', \phi) = q_{al} \int_{\mathbb{R}^2} \int_{-\pi}^{\pi} K_{al}^d(\vec{x} - \vec{s}) K_{al}^o(\theta; \phi') w_{al}(\phi' - \phi, \phi' - \theta) u(\vec{s}, \theta, t) d\theta d\vec{s}. \tag{2.22}$$

Similarly to T_a, both T_r and T_{al} have two kernels and one strength constant, q_j, each, which are identical to the ones defined in Equations (2.13) and (2.14). The w_r and w_{al} functions are defined through the same steps as Equations (2.18) - (2.20), with functions $g_{\sigma r}$, $g_{\sigma al}$, v_r and v_{al}, and with parameters k_r and k_{al}. There is, however, one major difference between T_r and T_a, and another major difference between T_{al} and T_a. The difference between T_r and T_a is that within the definition of w_r, the k_r must be between -1 and 0 instead of between 0 and 1. This is the only place the negative factor comes in to enforce the negative behaviour of the repulsion interaction. The attraction and alignment interactions are positive because they respond positively to the surrounding individuals.

The difference between T_{al} and T_a is ψ is replaced by θ in the definition of w_{al}. The alignment contribution to turning does not depend on the location of the neighbours, ψ, but rather on their direction, θ.

The reorientation rate T is more specific than λ because it accounts for every direction separately, while $\lambda(x, \phi)$ accounts for every direction at once. T and λ are actually related quite simply by

$$\lambda(\vec{x}, \phi) = \int_{-\pi}^{\pi} T(\vec{x}, \phi, \phi')d\phi'. \tag{2.23}$$

Notice ϕ and ϕ' have switched roles in T. Taking the integral over every turning rate in every possible direction, ϕ', gives the rate of turning in any direction. These are the definitions of T and λ respectively.

2.4 Model with a blind zone

In order to increase the biological realism of the model from Equation (2.1), proposed in [13], we introduce a blind zone. The model discussed in Sections 2.1 - 2.3 suggests that the neighbours behind an individual, when $\phi - \psi$ is close to $\pm\pi$, have the strongest influence on it. However, most animals cannot see behind themselves and are not susceptible to sudden changes occurring behind them, especially when animals depend primarily on sight. We require a blind zone that is in a consistent format to the model as it has been defined in Sections 2.1 - 2.3. Firstly, the blind zone is a kernel type that coincides with other kernels in how the integrals are computed. Secondly, the kernel has the ability to be fast Fourier transformed (FFT) without any complications. In other words, the kernel is periodic. Lastly, the kernel has convolution like qualities so as not to cause an increase in computational time. Discussion of these computational factors are discussed in Chapter 3. A blind zone kernel that meets all these requirements, shown in Figure 2.8, is

$$K_j^{bz}(\phi - \psi) = \frac{1}{B_j}\left(\frac{1}{2}\tanh\left\{c\left[\cos(\phi - \psi) + \left(1 - \frac{b}{\pi}\right)\right]\right\} + \frac{1}{2}\right), \tag{2.24}$$

where ϕ and ψ are the same as defined in Section 2.1, b determines the width of the blind zone, c the steepness of the blind zone, $j = a, r$ or al, and B_j is a constant that normalizes the kernel. Figure 2.8 shows how changing b and c can alter the blind zone.

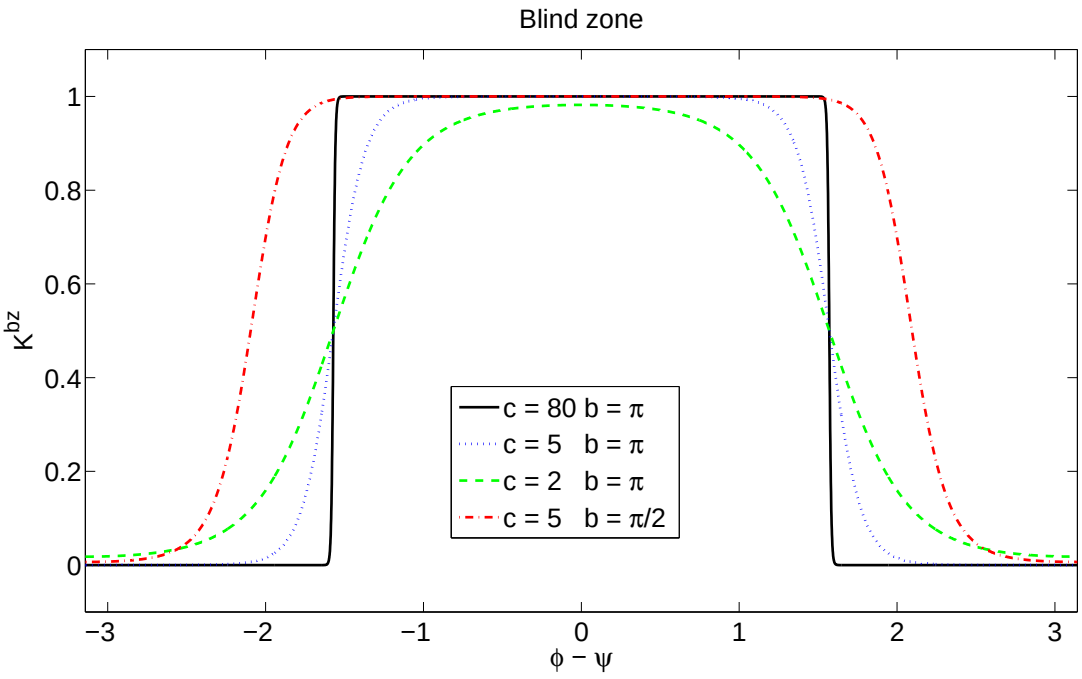

Figure 2.8: Blind zone: Four different blind zones for different values of c and b. Individuals in front are weighted more than individuals behind. This corresponds to a small $\phi - \psi$. The width of the blind zone is controlled by b, which can range from 0 to 2π. The steepness of the blind zone is controlled by c, which can range from 1 to ∞.

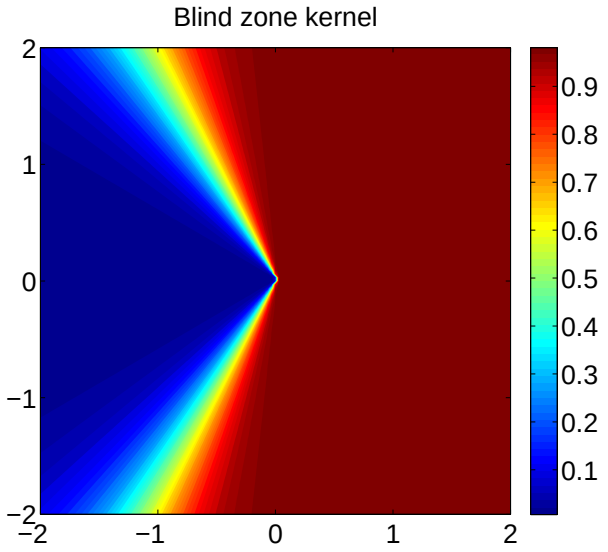

Figure 2.9: Blind zone kernel: This is the blind zone kernel from Equation (2.25). The individual is moving to the right and is influenced by the neighbours in front and to the sides, but is not influenced by neighbours behind. The blind zone kernel shown has parameter values of $b = \pi/2$ and $c = 5$, which are equivalent to those in Figure 2.8.

The kernel from Equation (2.24) can be transformed into

$$K_j^{bz}(\vec{s};\vec{x},\phi) = \frac{1}{B_j}\left(\frac{1}{2}\tanh\left\{c\left[-\cos\phi\frac{x_1-s_1}{|\vec{x}-\vec{s}|} - \sin\phi\frac{x_2-s_2}{|\vec{x}-\vec{s}|} + \left(1-\frac{b}{\pi}\right)\right]\right\} + \frac{1}{2}\right), \quad (2.25)$$

by using the cosine addition identity and simple trigonometry. Figure 2.9 shows the blind zone kernel with $\phi = 0$, which is when the individuals move to the right. The kernel from Equation (2.25) is added to the integral definitions of the λ's and the T's from Equations (2.12), (2.13), (2.14), (2.16), (2.21) and (2.22). They are now

$$\lambda_a(\vec{x},\phi) = q_a \int_{\mathbb{R}^2}\int_{-\pi}^{\pi} K_a^d(\vec{x}-\vec{s})K_a^{bz}(\vec{s};\vec{x},\phi)K_a^o(\vec{s};\vec{x},\phi)u(\vec{s},\theta,t)d\theta d\vec{s}, \quad (2.26)$$

$$\lambda_r(\vec{x},\phi) = q_r \int_{\mathbb{R}^2}\int_{-\pi}^{\pi} K_r^d(\vec{x}-\vec{s})K_r^{bz}(\vec{s};\vec{x},\phi)K_r^o(\vec{s};\vec{x},\phi)u(\vec{s},\theta,t)d\theta d\vec{s}, \quad (2.27)$$

$$\lambda_{al}(\vec{x},\phi) = q_{al} \int_{\mathbb{R}^2}\int_{-\pi}^{\pi} K_{al}^d(\vec{x}-\vec{s})K_{al}^{bz}(\vec{s};\vec{x},\phi)K_{al}^o(\theta;\phi)u(\vec{s},\theta,t)d\theta d\vec{s}, \quad (2.28)$$

$$T_a(\vec{x},\phi',\phi) = q_a \int_{\mathbb{R}^2}\int_{-\pi}^{\pi} K_a^d(\vec{x}-\vec{s})K_a^{bz}(\vec{s};\vec{x},\phi')K_a^o(\vec{s};\vec{x},\phi')w_a(\phi'-\phi,\phi'-\psi)u(\vec{s},\theta,t)d\theta d\vec{s}, \quad (2.29)$$

$$T_r(\vec{x},\phi',\phi) = q_r \int_{\mathbb{R}^2}\int_{-\pi}^{\pi} K_r^d(\vec{x}-\vec{s})K_r^{bz}(\vec{s};\vec{x},\phi')K_r^o(\vec{s};\vec{x},\phi')w_r(\phi'-\phi,\phi'-\psi)u(\vec{s},\theta,t)d\theta d\vec{s}, \tag{2.30}$$

$$T_{al}(\vec{x},\phi',\phi) = q_{al} \int_{\mathbb{R}^2}\int_{-\pi}^{\pi} K_{al}^d(\vec{x}-\vec{s})K_{al}^{bz}(\vec{s};\vec{x},\phi')K_{al}^o(\theta;\phi')w_{al}(\phi'-\phi,\phi'-\theta)u(\vec{s},\theta,t)d\theta d\vec{s}. \tag{2.31}$$

With the addition of the blind zone, the individuals do not react to neighbours behind them and this makes the model more realistic.

2.5 Conservation of Mass

In Section 3 of [13] properties of the model from Equation (2.1) are discussed. These properties are conservation of mass, boundedness of the solution and its gradient, positivity of the solution and global existence. These properties are taken to be true and will not be expanded on further, with the exception of conservation of mass which is discussed below.

When introducing the blind zone we want to ensure that mass is still conserved. To show this we must integrate both sides of Equation (2.1) over space and angle

$$\int_{\mathbb{R}^2}\int_{-\pi}^{\pi}(\partial_t u + \gamma\vec{e}_\phi\cdot\nabla_{\vec{x}}u)d\phi d\vec{s} = \int_{\mathbb{R}^2}\int_{-\pi}^{\pi} -\lambda(\vec{x},\phi)u + \int_{-\pi}^{\pi} T(\vec{x},\phi',\phi)u(\vec{x},\phi',t)d\phi' d\phi d\vec{s}. \tag{2.32}$$

The second term of the integrand, on the left hand side, goes to zero because the integral of $\nabla_{\vec{x}}u$ with respect to $\vec{s}$ is zero by the divergence theorem, since u vanishes at infinity. The first term of the integrand, on the left hand side, becomes

$$\partial_t \int_{\mathbb{R}^2}\int_{-\pi}^{\pi} u(\vec{s},\theta,t)d\theta d\vec{s}, \tag{2.33}$$

by bringing the derivative outside of the integral. Conservation of mass is true if integral (2.33) equals zero because the total density u does not change over time. To confirm that this is true, we need to verify that the right hand side of Equation (2.32) is zero, which is the same as showing

$$\int_{\mathbb{R}^2}\int_{-\pi}^{\pi}\lambda(\vec{x},\phi)u(\vec{x},\phi,t)d\phi d\vec{s} = \int_{\mathbb{R}^2}\int_{-\pi}^{\pi}\int_{-\pi}^{\pi} T(\vec{x},\phi',\phi)u(\vec{x},\phi',t)d\phi' d\phi d\vec{s}. \tag{2.34}$$

Since neither integrand depends on $\vec{s}$, the integrals over $\vec{s}$ can be ignored. The u term on the right hand side does not depend on ϕ, therefore we can bring the u out of the ϕ integral. Also, by changing the dummy variable on the left hand side from ϕ to ϕ' we have

$$\int_{-\pi}^{\pi}\lambda(\vec{x},\phi')u(\vec{x},\phi',t)d\phi' = \int_{-\pi}^{\pi} u(\vec{x},\phi',t)\int_{-\pi}^{\pi} T(\vec{x},\phi',\phi)d\phi d\phi'. \tag{2.35}$$

Since the integrands are equal, after eliminating the u factors, we have

$$\lambda(\vec{x}, \phi') = \int_{-\pi}^{\pi} T(\vec{x}, \phi', \phi) d\phi. \tag{2.36}$$

Expanding λ with Equation (2.11) and expanding T with Equation (2.15), Equation (2.36) becomes

$$\lambda_a(\vec{x}, \phi') + \lambda_r(\vec{x}, \phi') + \lambda_{al}(\vec{x}, \phi') = \int_{-\pi}^{\pi} [T_a(\vec{x}, \phi', \phi) + T_r(\vec{x}, \phi', \phi) + T_{al}(\vec{x}, \phi', \phi)] d\phi. \tag{2.37}$$

First, looking at attraction only, we have

$$\lambda_a(\vec{x}, \phi') = \int_{-\pi}^{\pi} T_a(\vec{x}, \phi', \phi) d\phi. \tag{2.38}$$

Using the definitions of λ_a and T_a, which are Equations (2.12) and (2.16), respectively, this becomes

$$q_a \int_{\mathbb{R}^2} \int_{-\pi}^{\pi} K_a^d(\vec{x} - \vec{s}) K_a^{bz}(\vec{s}; \vec{x}, \phi') K_a^o(\theta; \phi') u(\vec{s}, \theta, t) d\theta d\vec{s}$$

$$= \int_{-\pi}^{\pi} q_a \int_{\mathbb{R}^2} \int_{-\pi}^{\pi} K_a^d(\vec{x} - \vec{s}) K_a^{bz}(\vec{s}; \vec{x}, \phi') K_a^o(\theta; \phi') w_a(\phi' - \phi, \phi' - \theta) u(\vec{s}, \theta, t) d\theta d\vec{s} d\phi. \tag{2.39}$$

The only term which is dependent on ϕ is w_a. Bringing in the ϕ integral, all we are left to prove is that

$$\int_{-\pi}^{\pi} w_a(\phi' - \phi, \phi' - \theta) d\phi = 1. \tag{2.40}$$

This is the definition of the w terms from Equation (2.17). The same procedure from Equation (2.37) to (2.40) is repeatable for repulsion and alignment. Since the attraction, repulsion and alignment versions of Equation (2.40) hold, we know Equation (2.34) is true. This implies

$$\partial_t \int_{\mathbb{R}^2} \int_{-\pi}^{\pi} u(\vec{s}, \theta, t) d\theta d\vec{s} = 0, \tag{2.41}$$

and therefore mass is still conserved with the addition of the blind zone.

2.6 Predator

Though biological aggregates have interesting behaviours on their own, by introducing a predator, more dynamic behaviours are observable. Predators can influence prey movement by constricting prey into tighter groups, such as with dolphins [33] or minke whales [27] condensing fish into bait balls. Similarly predators can dive through a group and split the prey, such as an Eleonora's falcon

that dive bombs into a group of prey [18]. We are interested in observing the behaviour of the predator-prey relationship.

The predator's density, denoted u^h (h for hunter), is governed by similar equations to that of the prey, now denoted u^p. Akin to Equation (2.1), the two integro-differential equations for the prey and the predator are

$$\partial_t u^p + \gamma^p \vec{e}_\phi \cdot \nabla_{\vec{x}} u^p = -\lambda^p(\vec{x}, \phi) u^p + \int_{-\pi}^{\pi} T^p(\vec{x}, \phi', \phi) u^p(\vec{x}, \phi', t) d\phi', \tag{2.42}$$

$$\partial_t u^h + \gamma^h \vec{e}_\phi \cdot \nabla_{\vec{x}} u^h = -\lambda^h(\vec{x}, \phi) u^h + \int_{-\pi}^{\pi} T^h(\vec{x}, \phi', \phi) u^h(\vec{x}, \phi', t) d\phi', \tag{2.43}$$

where the speed that the predator travels is γ_h. Equations (2.42) and (2.43) are primary equations governing the movement of the predator and prey. The constants and functions with a p superscript in Equation (2.42) express the connection with the prey, while an h expresses the connection with the predator. Since there is now a predator in the model, the prey must respond by being repelled by the predator. Conversely, the predator is attracted to the prey.

Prey responds to predator

The constants and functions with a p superscript are the same as the ones in Equation (2.1), with the exception of the λ and the T functions. The difference between λ and λ^p is the extra contribution from the prey being repelled by the predator. Therefore we add λ^p_{rh} to the definition of λ and T^p_{rh} to the definition of T. Equations (2.11) and (2.15) become

$$\lambda^p(\vec{x}, \phi) = \lambda^p_a(\vec{x}, \phi) + \lambda^p_r(\vec{x}, \phi) + \lambda^p_{al}(\vec{x}, \phi) + \lambda^p_{rh}(\vec{x}, \phi), \tag{2.44}$$

$$T^p(\vec{x}, \phi', \phi) = T^p_a(\vec{x}, \phi', \phi) + T^p_r(\vec{x}, \phi', \phi) + T^p_{al}(\vec{x}, \phi', \phi) + T^p_{rh}(\vec{x}, \phi', \phi). \tag{2.45}$$

The superscripts indicate what type of population the function is connected to. The lack of a p or h in the subscripts indicates that the population interacts with itself, while a p or h in the subscript specifies that the superscript's population is being influenced by the subscript's population. For example, the functions λ^p_{rh} and T^p_{rh} are identical to λ^p_r and T^p_r, respectively, except instead of being repelled by u^p, the density of the prey on themselves, they are repelled by u^h, the density of the predators. The definitions of these functions are

$$\lambda^p_{rh}(\vec{x}, \phi) = q_{rh} \int_{\mathbb{R}^2} \int_{-\pi}^{\pi} K^d_{rh}(\vec{x} - \vec{s}) K^{bz}_{rh}(\vec{s}; \vec{x}, \phi) K^o_{rh}(\vec{s}; \vec{x}, \phi) u^h(\vec{s}, \theta, t) d\theta d\vec{s}, \tag{2.46}$$

$$T^p_{rh}(\vec{x},\phi',\phi) = q_{rh}\int_{\mathbb{R}^2}\int_{-\pi}^{\pi} K^d_{rh}(\vec{x}-\vec{s})K^{bz}_{rh}(\vec{s};\vec{x},\phi')K^o_{rh}(\vec{s};\vec{x},\phi')w_{rh}(\phi'-\phi,\phi'-\psi)u^h(\vec{s},\theta,t)d\theta d\vec{s}. \tag{2.47}$$

The $K^d_{rh}, K^{bz}_{rh}, K^o_{rh}$ and w_{rh} are analogous to the repulsion versions except that the constants are different values. These constants are A_{rh}, d_{rh}, m_{rh}, q_{rh} and k_{rh}. The definitions of the other six functions from Equations (2.44) and (2.45) are the same as the functions without the p superscripts from Equations (2.12), (2.13), (2.14), (2.16), (2.21) and (2.22).

Predator responds to itself and to the prey

The predator is attracted to and repelled from itself, however it does not align with itself. The absence of alignment for the predator decreases the computation time of the code, which is discussed further in Chapter 3. The predator is attracted to the prey, and this behaviour is captured by λ^h_{ap} and T^h_{ap}. Therefore the λ^h and the T^h for the predator is

$$\lambda^h(\vec{x},\phi) = \lambda^h_a(\vec{x},\phi) + \lambda^h_r(\vec{x},\phi) + \lambda^h_{ap}(\vec{x},\phi), \tag{2.48}$$

$$T^h(\vec{x},\phi',\phi) = T^h_a(\vec{x},\phi',\phi) + T^h_r(\vec{x},\phi',\phi) + T^h_{ap}(\vec{x},\phi',\phi). \tag{2.49}$$

The λ^h_a and T^h_a denote the attraction the predator has with itself. The λ^h_r and T^h_r denote the repulsion the predator has with itself. The λ^h_{ap} and T^h_{ap} denote the attraction the predator has towards the prey. These six functions are defined by

$$\lambda^h_a(\vec{x},\phi) = \bar{q}_a\int_{\mathbb{R}^2}\int_{-\pi}^{\pi} \bar{K}^d_a(\vec{x}-\vec{s})\bar{K}^{bz}_a(\vec{s};\vec{x},\phi)\bar{K}^o_a(\vec{s};\vec{x},\phi)u^h(\vec{s},\theta,t)d\theta d\vec{s}, \tag{2.50}$$

$$\lambda^h_r(\vec{x},\phi) = \bar{q}_r\int_{\mathbb{R}^2}\int_{-\pi}^{\pi} \bar{K}^d_r(\vec{x}-\vec{s})\bar{K}^{bz}_r(\vec{s};\vec{x},\phi)\bar{K}^o_r(\vec{s};\vec{x},\phi)u^h(\vec{s},\theta,t)d\theta d\vec{s}, \tag{2.51}$$

$$\lambda^h_{ap}(\vec{x},\phi) = \bar{q}_{ap}\int_{\mathbb{R}^2}\int_{-\pi}^{\pi} \bar{K}^d_{ap}(\vec{x}-\vec{s})\bar{K}^{bz}_{ap}(\vec{s};\vec{x},\phi)\bar{K}^o_{ap}(\vec{s};\vec{x},\phi)u^p(\vec{s},\theta,t)d\theta d\vec{s}, \tag{2.52}$$

$$T^h_a(\vec{x},\phi',\phi) = \bar{q}_a\int_{\mathbb{R}^2}\int_{-\pi}^{\pi} \bar{K}^d_a(\vec{x}-\vec{s})\bar{K}^{bz}_a(\vec{s};\vec{x},\phi)\bar{K}^o_a(\vec{s};\vec{x},\phi)\bar{w}_a(\phi'-\phi,\phi'-\psi)u^h(\vec{s},\theta,t)d\theta d\vec{s}, \tag{2.53}$$

$$T^h_r(\vec{x},\phi',\phi) = \bar{q}_r\int_{\mathbb{R}^2}\int_{-\pi}^{\pi} \bar{K}^d_r(\vec{x}-\vec{s})\bar{K}^{bz}_r(\vec{s};\vec{x},\phi)\bar{K}^o_r(\vec{s};\vec{x},\phi)\bar{w}_r(\phi'-\phi,\phi'-\psi)u^h(\vec{s},\theta,t)d\theta d\vec{s}, \tag{2.54}$$

$$T^h_{ap}(\vec{x},\phi',\phi) = \bar{q}_{ap}\int_{\mathbb{R}^2}\int_{-\pi}^{\pi} \bar{K}^d_{ap}(\vec{x}-\vec{s})\bar{K}^{bz}_{ap}(\vec{s};\vec{x},\phi)\bar{K}^o_{ap}(\vec{s};\vec{x},\phi)\bar{w}_{ap}(\phi'-\phi,\phi'-\psi)u^p(\vec{s},\theta,t)d\theta d\vec{s}, \tag{2.55}$$

where the bars denote that they correspond to the predator. With the formulation of the predator's equations, the $\bar{K}$'s, $\bar{w}$'s, λ^h's and T^h's have constants $\bar{A}_a, \bar{A}_r, \bar{A}_{ap}, \bar{d}_a, \bar{d}_r, \bar{d}_{ap}, \bar{m}_a, \bar{m}_r, \bar{m}_{ap}$, $\bar{q}_a, \bar{q}_r, \bar{q}_{ap}, \bar{k}_a, \bar{k}_r$ and $\bar{k}_{ap}$ analogous to the constants for the prey.

With any addition to this model one needs to check conservation of mass. It will be conserved provided all of

$$\lambda^p_{rh}(\vec{x}, \phi') = \int_{-\pi}^{\pi} T^p_{rh}(\vec{x}, \phi', \phi) d\phi. \tag{2.56}$$

$$\lambda^h_{a}(\vec{x}, \phi') = \int_{-\pi}^{\pi} T^h_{a}(\vec{x}, \phi', \phi) d\phi. \tag{2.57}$$

$$\lambda^h_{r}(\vec{x}, \phi') = \int_{-\pi}^{\pi} T^h_{r}(\vec{x}, \phi', \phi) d\phi. \tag{2.58}$$

$$\lambda^h_{ap}(\vec{x}, \phi') = \int_{-\pi}^{\pi} T^h_{ap}(\vec{x}, \phi', \phi) d\phi. \tag{2.59}$$

hold. This follows the same procedure of Equations (2.38) - (2.40) except using different subscripts.

The above description adds a predator to create a predator-prey relationship. This model, using very similar ideas, can be altered to describe different types of relationships. Two-species interacting may not be necessarily of a predator-prey type. They could, for instance, compete for the same resources, but at the same time avoid each other. Alternatively, another stationary predator could be added that might act as an obstacle. In theory, this model could extend to any number of species that have a variety of relationships with other species. However, our research only focuses on the single predator and single prey relationship.

Chapter 3

Numerical Method

We use the fourth order Runge-Kutta spectral method to progress the population density in time. The spatial dimension has N^2 points with a square domain of a side length of L, which goes from $[-\frac{L}{2}, \frac{L}{2})$ on both the x and y axes. The spatial grid spacing is $\Delta x = \Delta y = \frac{L}{N}$. The angle dimension has M points with a domain of 2π radians, which goes from $[-\pi, \pi)$, with grid spacing of $\Delta\phi = \frac{2\pi}{M}$.

To avoid aliasing the spatial grid is extended from N^2 to $(\frac{3}{2}N)^2$ and the angular grid is extended from M to $\frac{3}{2}M$. The $\frac{3}{2}$ is the smallest possible factor to guarantee that dealiasing is successful and to minimize the computational time. Some functions with this spatial and angular extension are fast Fourier transformed into the Fourier space, and then have the highest third of the frequency Fourier coefficients set to zero. The calculations are carried out in the extended real and frequency domains, and then it is reduced back to the original size. This dealiasing process is standard as discussed in [5].

The left hand side of the integro-differential equations (Equations (2.42) and (2.43)) can be updated by first taking the 2D Fourier transform of the linear convective term, which becomes

$$\gamma \left(\cos\phi \, l_1 + \sin\phi \, l_2\right) \hat{u}, \tag{3.1}$$

where l_1 is the horizontal component of the wave number and l_2 is the vertical. This new algebraic form for the left hand side of Equations (2.42) and (2.43) can now be computed using the integrating factor technique.

The right hand side of the integro-differential equations (Equations (2.42) and (2.43)) requires

much more work than the left hand side. The right hand side requires the computations of integrals to calculate λ and T. The calculation of these integrals are done via convolutions in Fourier space, which are calculated significantly faster in comparison to other methods, such as quadrature methods. Convolutions in Fourier space are calculated by multiplication as opposed to an integral calculation in real space. Both spatial and angle components of some λ's and T's can be convolved but some cannot. The ones that cannot will be calculated using a quadrature method. For example, the λ_{al} function,

$$\lambda_{al}(\vec{x},\phi) = q_{al}\int_{\mathbb{R}^2} K^d_{al}(\vec{x}-\vec{s})K^{bz}_{al}(\vec{s};\vec{x},\phi)\int_{-\pi}^{\pi} K^o_{al}(\theta;\phi)u(\vec{s},\theta,t)d\theta d\vec{s}, \tag{3.2}$$

has the integral over θ as a convolution in angle (see Equation (2.10)). Therefore, the K^o_{al} and the u terms can be Fourier transformed and then multiplied together. This product must then be inverse Fourier transformed. The remaining space integral can be calculated via convolution in $\vec{s}$, where K^{bz}_{al} is a function of $\vec{x}-\vec{s}$. The design of the blind zone allows it to be multiplied with K^d_{al} before the spatial convolution with u. This addition of the blind zone increases the computational time by a very slight amount. The T_{al} function,

$$T_{al}(\vec{x},\phi',\phi) = q_{al}\int_{\mathbb{R}^2} K^d_{al}(\vec{x}-\vec{s})K^{bz}_{al}(\vec{s};\vec{x},\phi')\int_{-\pi}^{\pi} K^o_{al}(\theta;\phi')w_{al}(\phi'-\phi,\phi'-\theta)u(\vec{s},\theta,t)d\theta d\vec{s}, \tag{3.3}$$

does not have the luxury of using a convolution to compute the integral over θ because both K^o_{al} and w_{al} are dependent on $\phi'-\theta$ (see Equations (2.10) and (2.18)). The integral over θ is calculated using the trapezoidal rule with a double for loop, which is computationally taxing. The integral over $\vec{s}$ can still be easily calculated in the same manner as the λ_{al} case. However, the integral over θ for the T_{al} function takes up so much time computationally that we have excluded the alignment terms in the derivation of the evolution of the predator to help increase the computational speed. This has lowered the computational cost by slightly less than a factor of two.

From Equations (2.44) and (2.48), the attraction and repulsion components of all six other λ's are

$$\lambda^i_j(\vec{x},\phi) = q_j\int_{\mathbb{R}^2} K^d_j(\vec{x}-\vec{s})K^{bz}_j(\vec{s};\vec{x},\phi)K^o_j(\vec{s};\vec{x},\phi)\int_{-\pi}^{\pi} u^i(\vec{s},\theta,t)d\theta d\vec{s}, \tag{3.4}$$

where $i = p$ or h, and where $j = a$, r, rh or ap. Note that the alignment has been excluded. In each case the K^d, K^o and K^{bz} kernels are multiplied together and are then convolved with the u function. Before this happens, the integral over θ must be calculated. This integral is equal to the zero-mode of u with respect to angle. Therefore, we Fourier transformed u, took the zeroth coefficient of u and

convolved this coefficient with the kernels in the integral over $\vec{s}$. Equations (2.7), (2.9) and (2.25) remind us how the K^o and K^{bz} kernels are functions of $\vec{x} - \vec{s}$.

From Equations (2.45) and (2.49), the attraction and repulsion components for all six other T's are

$$T_j^i(\vec{x}, \phi', \phi) = q_j \int_{\mathbb{R}^2} K_j^d(\vec{x} - \vec{s}) K_j^{bz}(\vec{s}; \vec{x}, \phi') K_j^o(\vec{s}; \vec{x}, \phi') w_j(\phi' - \phi, \phi' - \psi) \int_{-\pi}^{\pi} u^i(\vec{s}, \theta, t) d\theta d\vec{s}, \tag{3.5}$$

where i = p or h, and where j = a, r, rh or ap. Note that, again, the alignment has been excluded. The calculation of the different T's in Equation (3.5) is similar to the λ's in Equation (3.4) except there is an extra w_j term. The w_j can also be thought of as a function of $\vec{x} - \vec{s}$ after fixing ϕ and ϕ' and after the following steps

$$\begin{aligned} w_j\left(\phi' - \phi, \phi' - \psi\right) &= g_{\sigma_j}\left(\phi' - \phi - \kappa_j \sin\left(\phi' - \psi\right)\right) \\ &= g_{\sigma_j}\left(\phi' - \phi - \kappa_j \left(\sin\phi' cos\psi - \cos\phi' sin\psi\right)\right) \\ &= g_{\sigma_j}\left(\phi' - \phi - \kappa_j \left(\sin\phi' \frac{s_x}{s_x^2 + s_y^2} - \cos\phi' \frac{s_y}{s_x^2 + s_y^2}\right)\right). \end{aligned}$$

Since the w_j's are functions of $\vec{x} - \vec{s}$, they can be multiplied with the kernels before the convolution over $\vec{s}$, making for a much quicker calculation compared to T_{al}. With all the λ's and T's calculated, the right hand side of Equations (2.42) and (2.43) can be calculated by some simple matrix calculations.

Chapter 4

Numerical Experiments

The following chapter showcases the versatility of the model and how it captures both interactions among a solitary group of prey and interactions between predator and prey. For all experiments we take the size of the domain, $L = 4$, the speed of the prey, $\gamma = 1$, and $\sigma = 0.2$ from Equation (2.19). The parameters defining the size and location of the kernels are also set for all experiments: $d_r = 0$, $d_{al} = 0.4$, $d_a = 0.8$, $m_r = m_{al} = m_a = 0.2$. The parameters controlling the blind zone are also fixed, with $c = 10$ and $b = \frac{\pi}{2}$, except for the blind zone experiments, which show the effect of changing the blind zone. Once the predator is introduced, there are some other fixed parameters. These are $d_{rh} = 0, m_{rh} = 0.8, \bar{d}_r = 0, \bar{m}_r = 0.2, \bar{d}_a = 0.4, \bar{m}_a = 0.2, \bar{d}_{ap} = 0.4$ and $\bar{m}_{ap} = 0.4$. The bar represents that these constants refer to the predator. For example, the m_r shows the width of the zone of influence for the prey being repelled by itself, the m_{rh} shows this width for the prey being repelled by the predator, and $\bar{m}_r$ shows this width for the predator being repelled by itself. In Section 4.1, a model without a predator is showcased. In Section 4.2, simulations for the stationary predator model is shown. The moving predator model will be implemented in Section 4.3 and the turning predator model will be implemented in Section 4.4.

4.1 Prey

In this section, behaviour of prey without predators is studied. Modeling the behaviour of prey in the absence of a predator produces interesting and complex patterns. Additionally, it allows for

the model with a predator to be validated by insuring that the model without the predator accurately depicts normal behaviour of aggregations. We first show some expected behaviours of the prey in the absence of a predator. In [13] there were three basic behaviours showcased: stationary aggregation, translating uniform aggregation, and moving aggregation with alignment. Adding to these experiments, we have experiments called oval swarm, collision of two groups, cluster size and milling.

4.1.1 Oval swarm

The initial condition for the population density is a random distribution in space and angle. The parameters describing the strength of interactions are $q_r = 3.4410$, $q_{al} = 0.4986$ and $q_a = 2.9311$. The proportionality constants that depict the amount of turning are $k_r = -0.0519$, $k_{al} = 0.9957$ and $k_a = 0.8779$. During the simulation, the prey congregate at one location (see Figure 4.1). With q_r being the highest, one would expect the individuals never to form a group. However, since k_r is low, the individuals cannot turn quickly and the group is more influenced by attraction. Subsequently, the combination of q_a and k_a is stronger than the combination of q_r and k_r, therefore the individuals form a group. The slight difference between q_r and q_a will eventually be enough to make the group split. Figure 4.1 has small white arrows which show the average direction an individual located at a given grid point is moving in, and the size of the arrows shows the relative amount of motion of the individuals. Looking at the directions, one can notice that there is a complicated way in which the individuals move around. They move into the group from the left and right, and they move out of the group from the top and bottom. This model has also captured a four-in-four-out system, seen in Figure 4.7. After some time the group slowly becomes a flattened oval shaped.

4.1.2 Collision of two groups

In this experiment two small groups of individuals collide and travel in a direction that is half way between the original directions of the two groups. One group travels horizontally to the right, while the other moves vertically upward. They collide at (0,0) and move equally upward and to the right (see Figure 4.2). This is a classic case of conservation of momentum. The parameters used in this experiment are $q_r = 1$, $q_{al} = 90$, $q_a = 90$, $k_r = -0.25$, $k_{al} = 0.75$ and $k_a = 0.25$. The decision to make q_a and q_{al} large allows for a successful merger. If these parameters were smaller, the two

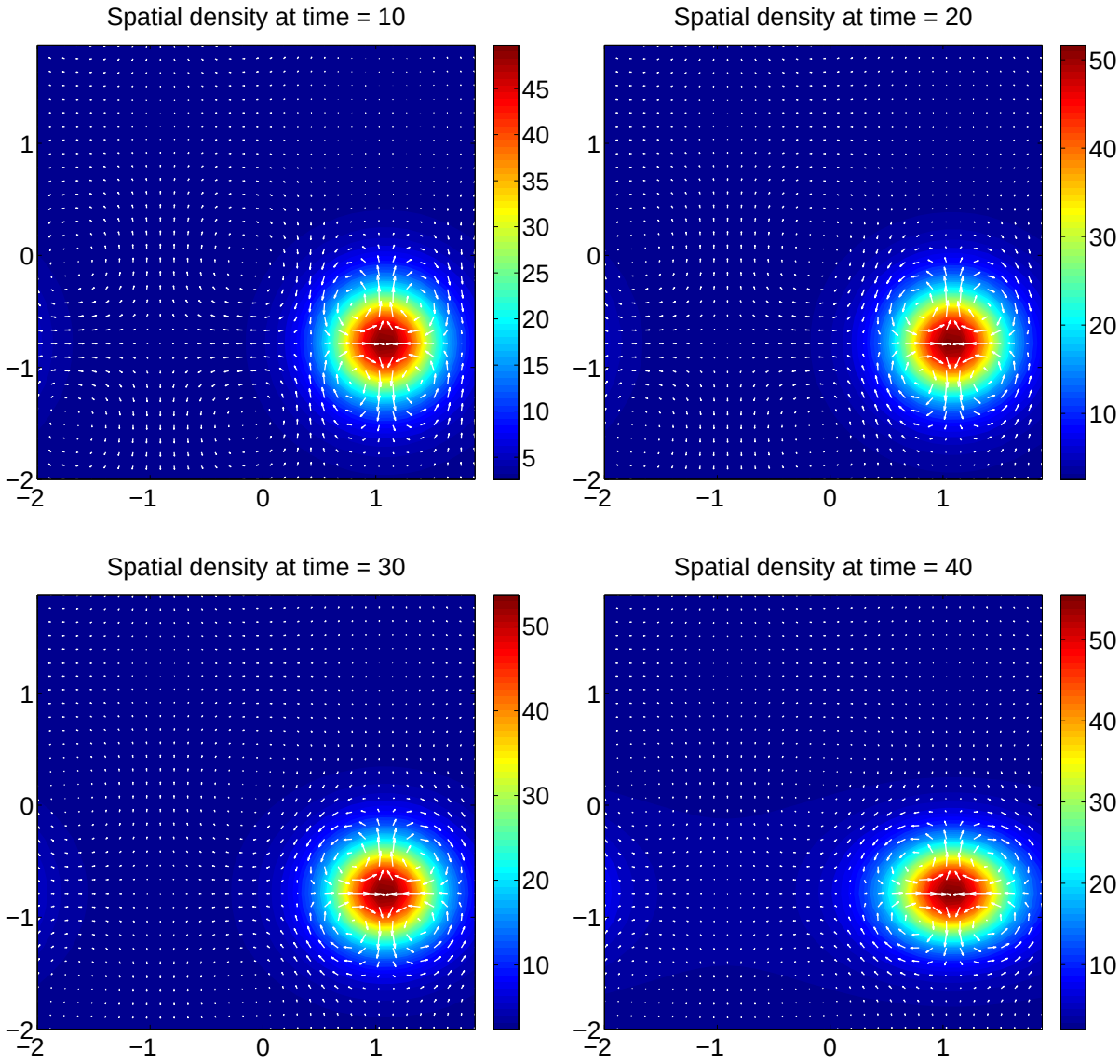

Figure 4.1: Oval swarm: The combination of $q_a = 2.9311$ and $k_a = 0.8779$ is stronger than the combination of $q_r = 3.4410$ and $k_r = -0.051$, therefore the individuals form a circular group and it slowly turns into an oval because of the internal flow of individuals, shown by the white arrows.

original groups would be more inclined to travel through each other, with only slight interaction. There is a middle range as well, with the two original groups travelling through each other but having some individuals fan out in an arc connecting the two groups after collision, which is not shown here.

4.1.3 Cluster size

In this experiment, two identical simulations are done except one has twice the amount of individuals (see Figure 4.3). The initial conditions are a random distribution in space and angle. The parameters used in this experiment are $q_r = 1$, $q_{al} = 5$, $q_a = 5$, $k_r = -0.1$, $k_{al} = 0.75$ and $k_a = 0.75$. These are the same parameters for "Run 3", a moving aggregation with alignment, in [13], which depicts a group of individuals moving in a particular direction with a tail. The plot on the left in Figure 4.3 shows the moving group with a tail. This group is more oval shaped compared to the one in [13] likely because our version has a blind zone, which is the only difference between the two models. Some fish, such as cod, can school in a ratio of length:width:depth ratio ranging from 10:4:1 to 2:4:1 (see [3]). Figure 4.3 shows a 2:3 length to width ratio (depth would be the third dimension, not done in this model).

One advantage of grouping in a more oval shape is the distance of the common blind zone away from the group. For a solitary individual, the blind zone is directly behind it. For a group, however, the peripheral sight lines of each individual overlap with the blind zones of their side neighbours. This creates a common blind zone that is located at a distance from the group instead of directly behind it, as discussed in [28] (see Figure 4.4). An oval shape helps to increase the distance of the common blind zone away from the group.

The plot on the right of Figure 4.3 has twice the initial population than the plot on the left. Notice, however, that the spatial size of the groups is the same, meaning that the density of the group on the right is double that of the group on the left. This makes sense mathematically, though not biological because the group usually plateaus at a maximum density. As discussed in [25, 30], sharp boundaries and relatively constant internal population densities are hard to capture in models. More work is required to capture these biologically realistic behaviours.

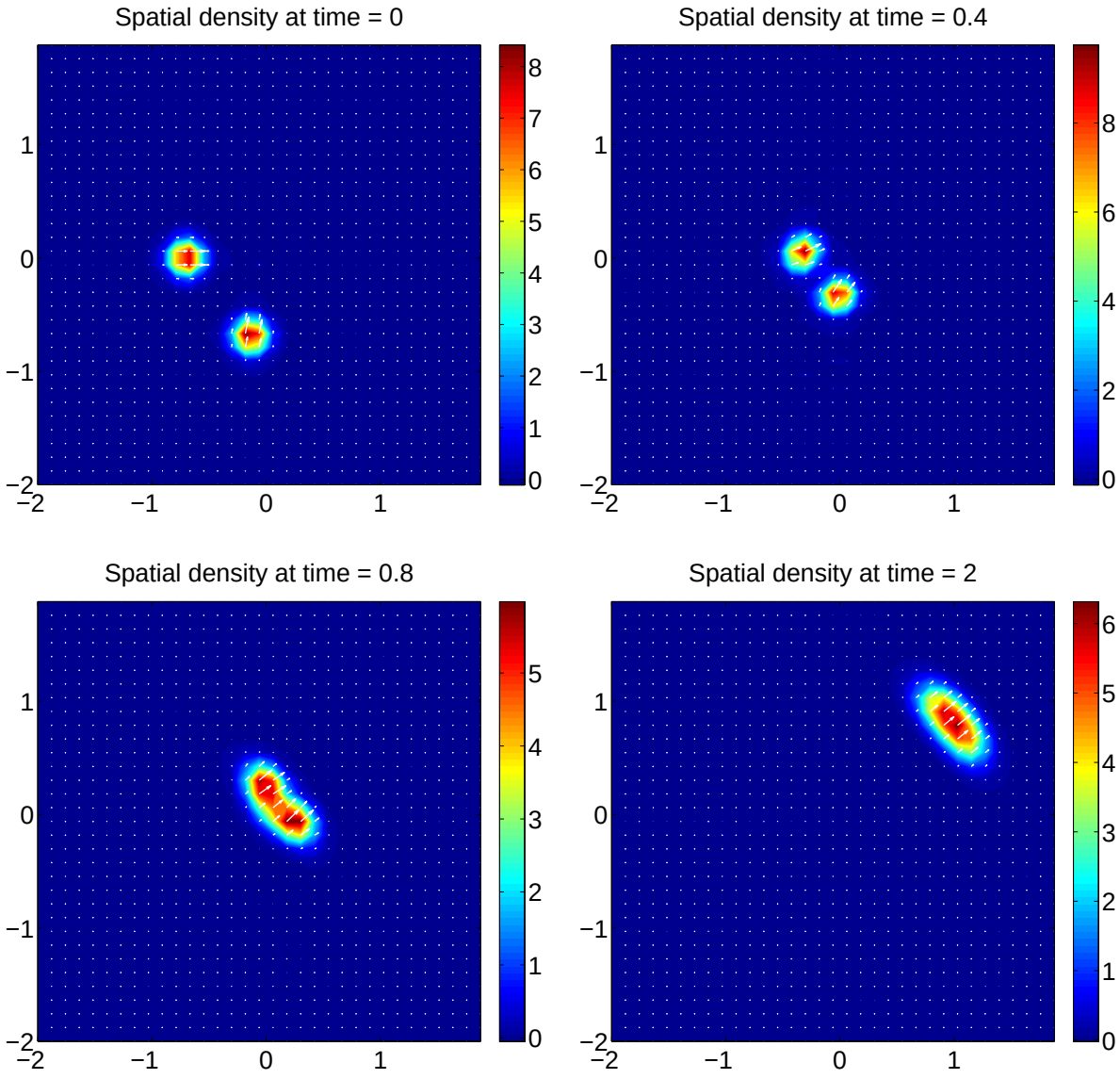

Figure 4.2: Collision of two groups: Two masses of equal size run into each other perpendicularly. They merge and travel in a 45 degree angle.

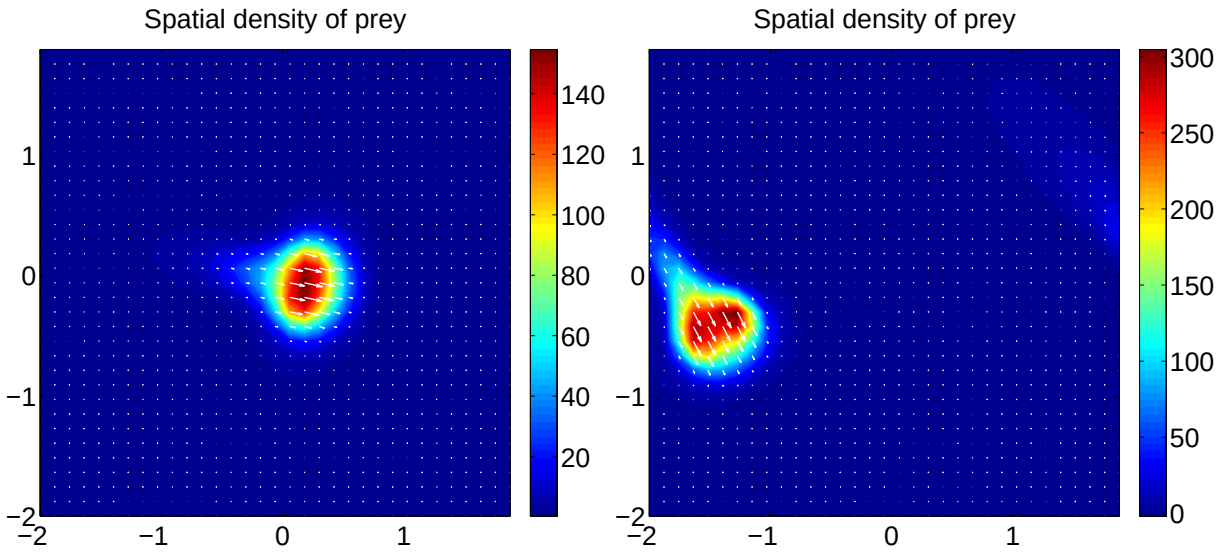

Figure 4.3: Cluster size: The group on the right has twice as many individuals as the group on the left. Doubling the amount of individuals creates a group that has double the density.

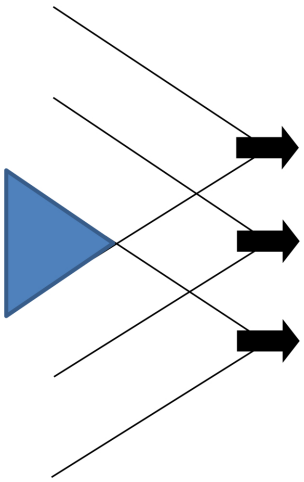

Figure 4.4: Common blind zone: The peripheral sight lines of three individuals are shown. The common blind zone of all three individuals in shown by the triangle, which is further from a given individual compared to its own blind zone.

Figure 4.5: Milling: Milling behaviour of bluefin tuna. The image is from http://www.nationalgeographic.com.

4.1.4 Milling

In this experiment the individuals attempt to maintain a milling formation that was initiated from the initial conditions (see Figures 4.5 and 4.6). The individuals move around in a annular shape, and are influenced to turn to maintain this shape because of individuals in front and on the opposite side of the annulus. Unfortunately, a true milling pattern was not achieved because the individuals would either spread out or converge in. Figure 4.6 shows a spreading out over time. The centripetal force required to keep the individuals in a stable mill needs to come from the attraction parameters. If the individuals move away from the centre, the attraction force decreases and the individuals continue to move away. Conversely, if the individuals move towards the centre, the attraction force becomes larger and the individuals will collapse into a ball. We believe a more extensive parameter search would uncover this pattern.

The parameters used in this experiment are $q_r = 4$, $q_{al} = 6$, $q_a = 5$, $k_r = -0.25$, $k_{al} = 0.75$ and $k_a = 0.25$. Some other parameters that are usually fixed were changed: $d_{al} = 0.2$, $m_a = 0.5$, $m_r = 0.1$ and $m_{al} = 0.1$. These changes make the width of the repulsion zone smaller, the width and radius of the alignment zone smaller and the width of the attraction zone larger. The parameters were changed because of an idea from [9]. The idea is that the individuals align themselves with neighbours in front of them, while the individuals will be attracted to others on the opposite side

of the milling annulus. What is important here is that the alignment zone is small enough so the individuals do not align themselves with individuals on the other side of the annulus.

In [9], a particle-based model was used to show a milling formation in an aggregation. In [20], a Lagrangian model based on Newton's equations of motion was used to study milling formations and their existence, while keeping track of the group radius and the individuals' angular velocity. Milling in a torus is a common phenomenon in fish, such as tuna, jack and barracuda [9].

4.2 Stationary predator

In this section, we introduce a stationary predator, which the prey are repelled by. Since the predator is stationary, the equations governing the movement of the predator are not included in the simulation. Therefore the equation for λ^p (Equation (2.44)) will now have the λ^p_{rh} component, but Equations (2.43), (2.48) and (2.49) are not needed.

4.2.1 Prey near a predator and food

All animals behave in such a way as to avoid predation. In order to avoid the predator, prey rely on interactions with their neighbours as well as interactions with the predator. The left plot in Figure 4.7 shows the prey's behaviour with the predator centred at $(0.5, 0)$, with the predator's spatial density

$$u^h = 5e^{-\left(\frac{(x-0.5)^2+y^2}{0.05}\right)}. \tag{4.1}$$

The parameters used in this experiment are $q_r = 4$, $q_{al} = 3$, $q_a = 3$, $q_{rh} = 50$, $k_r = -0.65$, $k_{al} = 0.85$, $k_a = 0.85$ and $k_{rh} = -0.99$. The repulsion magnitude is slightly larger than the alignment and attraction ones. In the absence of the predator, this would cause the prey to disperse to a uniform state, but with the predator the prey congregate to the area which is the furthest away from the predator. The white arrows in the left plot of Figure 4.7 show a four-in-four-out system of movement. This is probably caused by the square shaped domain. Also, the arrow size is relative to the magnitude of motion of individuals in a particular simulation. Though they may appear similar in size by arrows in other simulations the actual magnitude is not the same. In the case Figure 4.7,

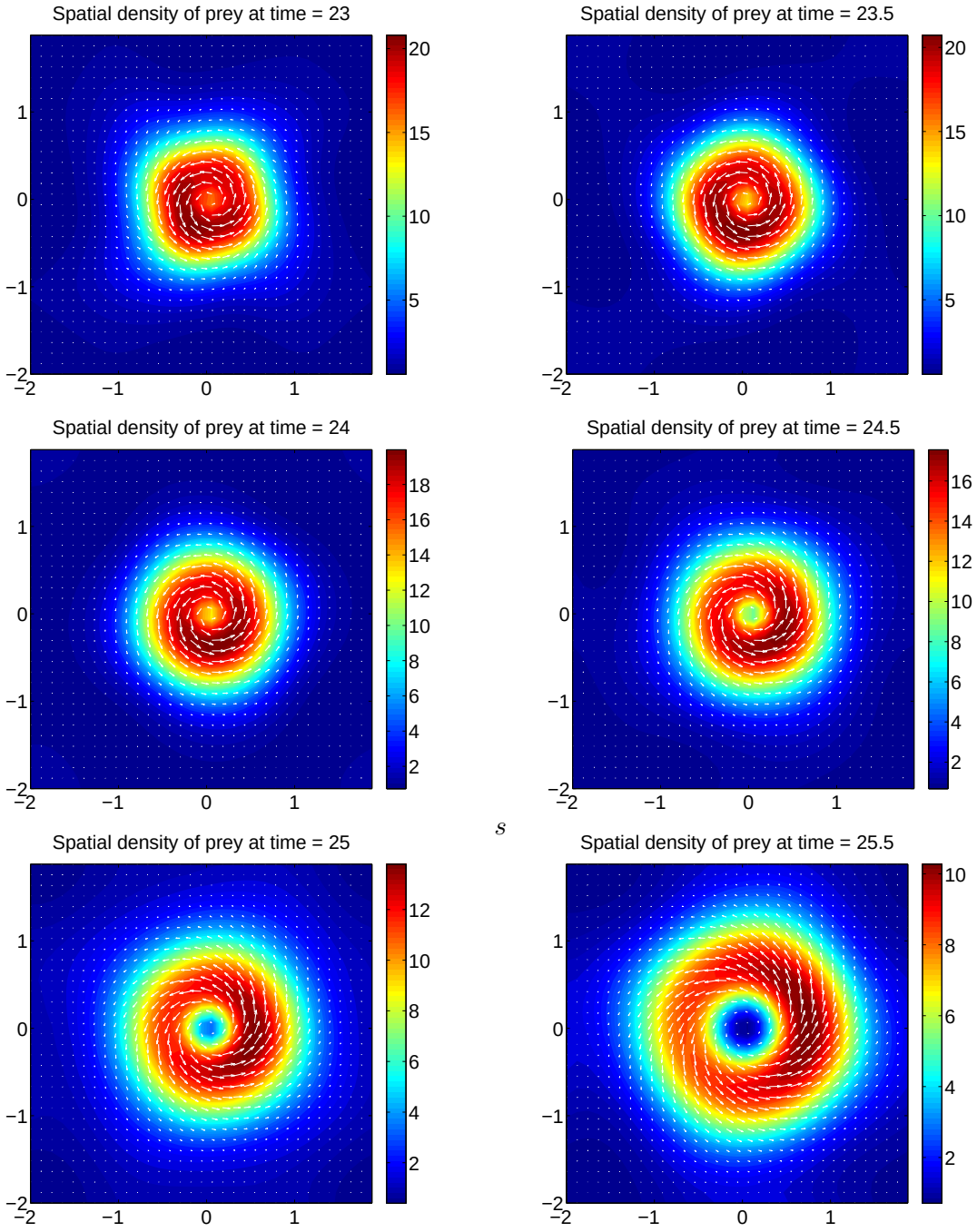

Figure 4.6: Milling: Milling like behaviour is maintained for a small amount of time.

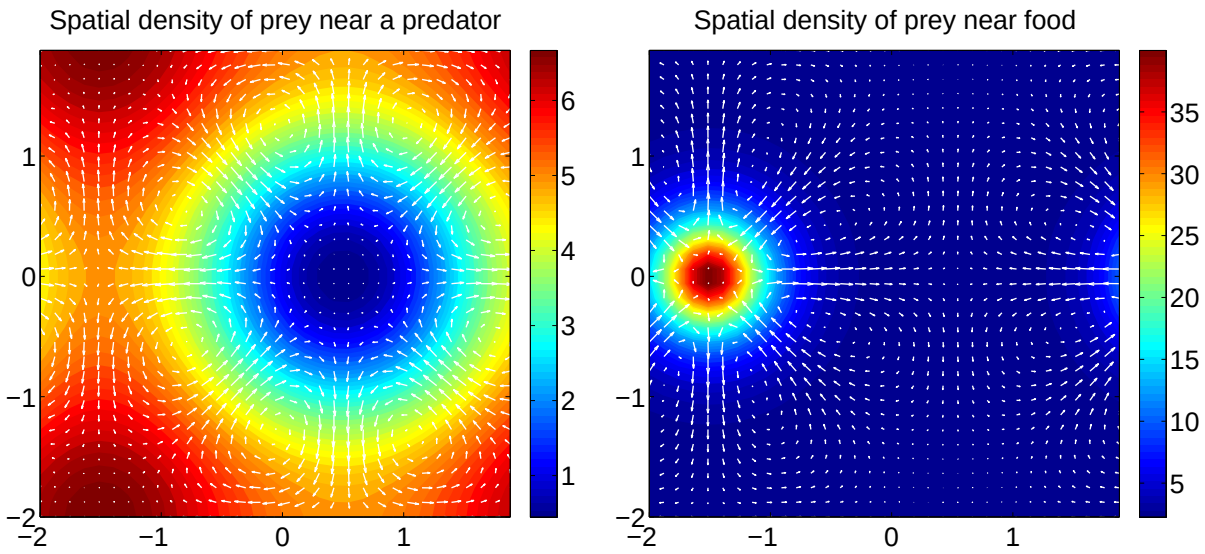

Figure 4.7: Prey near a predator and food: The prey are repelled by the predator, centered at (0.5,0), and attracted to the food centered at (-1.5,0), each simulated separately. All parameters are kept the same except the amplitudes of each of the predator, left, and the food, right.

the arrows are large even though there is very little movement of the individuals.

The model can easily be switched to prey moving towards a stationary food source. The right plot in Figure 4.7 shows the prey's behaviour with food centred at $(-1.5, 0)$, with the food's spatial density

$$u^F = 5e^{-\left(\frac{(x+1.5)^2+y^2}{0.05}\right)}, \tag{4.2}$$

where the F stand for food. Prey in this case congregate quickly around the food. The prey in the right plot of Figure 4.7 show a four-in-four-out system similar to the one discussed above. The parameters are $q_r = 4$, $q_{al} = 3$, $q_a = 3$, $q_{rF} = 50$, $k_r = -0.65$, $k_{al} = 0.85$, $k_a = 0.85$ and $k_{rF} = 0.99$ and the population of the predator is now zero and the population of the food is now non-zero. This is the only time food is considered and will not be discussed further.

These experiments depict behaviour of prey in the natural world. In order to survive, individuals must make it their priority to find food and avoid predators.

4.2.2 Prey avoiding a predator

An aggregation of prey avoiding a predator remains as a group. The group of prey are deflected by the predator, as seen in Figure 4.8. The predator is stationary as shown in the top left of Figure 4.8. The other five plots show the prey coming towards the predator and turning to avoid it.

The parameters used in this experiment are $q_r = 1$, $q_{al} = 3$, $q_a = 3$, $q_{rh} = 50$, $k_r = -0.25$, $k_{al} = 0.85$, $k_a = 0.85$ and $k_{rh} = -0.99$. The strength of q_r is significantly reduced in comparison to Section 4.2.1, which causes the prey to congregate instead of disperse. The q_{rh} is high making the predator affect the prey significantly. With k_{rh} being very close to -1, the prey respond to the predator rapidly.

In this experiment the prey will not only move away from the predator, they will also stay together as a group while doing so. The stationary predator can be viewed as an obstacle, provided the repulsion parameters are large enough to ensure that the prey cannot move through the obstacle. For example, migratory animals, such as caribou, are diverted around lakes. Since caribou will walk around a lake migrating, it can be thought of as the caribou being repelled by the lake.

4.2.3 Predator ring

Predators sometimes cannot rely on speed and agility to catch their prey. Therefore, predators must come up with clever ways to catch their prey which take less effort and are more efficient. One such method is the predator ring. The predators surround the prey, forcing it into a ball, which condenses the group. This increases the probability of the predator catching its prey. Figure 4.10 shows the predator ring in the top left figure, and five plots of the prey moving around in the ring.

The parameters for this experiment are $q_r = 4$, $q_{al} = 5$, $q_a = 1$, $q_{rh} = 20$, $k_r = -0.65$, $k_{al} = 0.85$, $k_a = 0.85$ and $k_{rh} = -0.7$. The m_{rh} parameter was changed from 0.8 to 0.6 in this experiment to allow the prey to get closer to the predators, which does not confine it too much to the centre of the ring. The prey's initial condition is a small counter-clockwise rotating ball which eventually spreads apart. Because of this initial condition, the prey deflects off of the predator ring and continues in a counter-clockwise rotation.

The behaviour of a predator ring is found in nature in a variety of forms. Two such forms are that of dolphins [33] and minke whales [27] condensing fish into bait balls (see Figure 4.9).

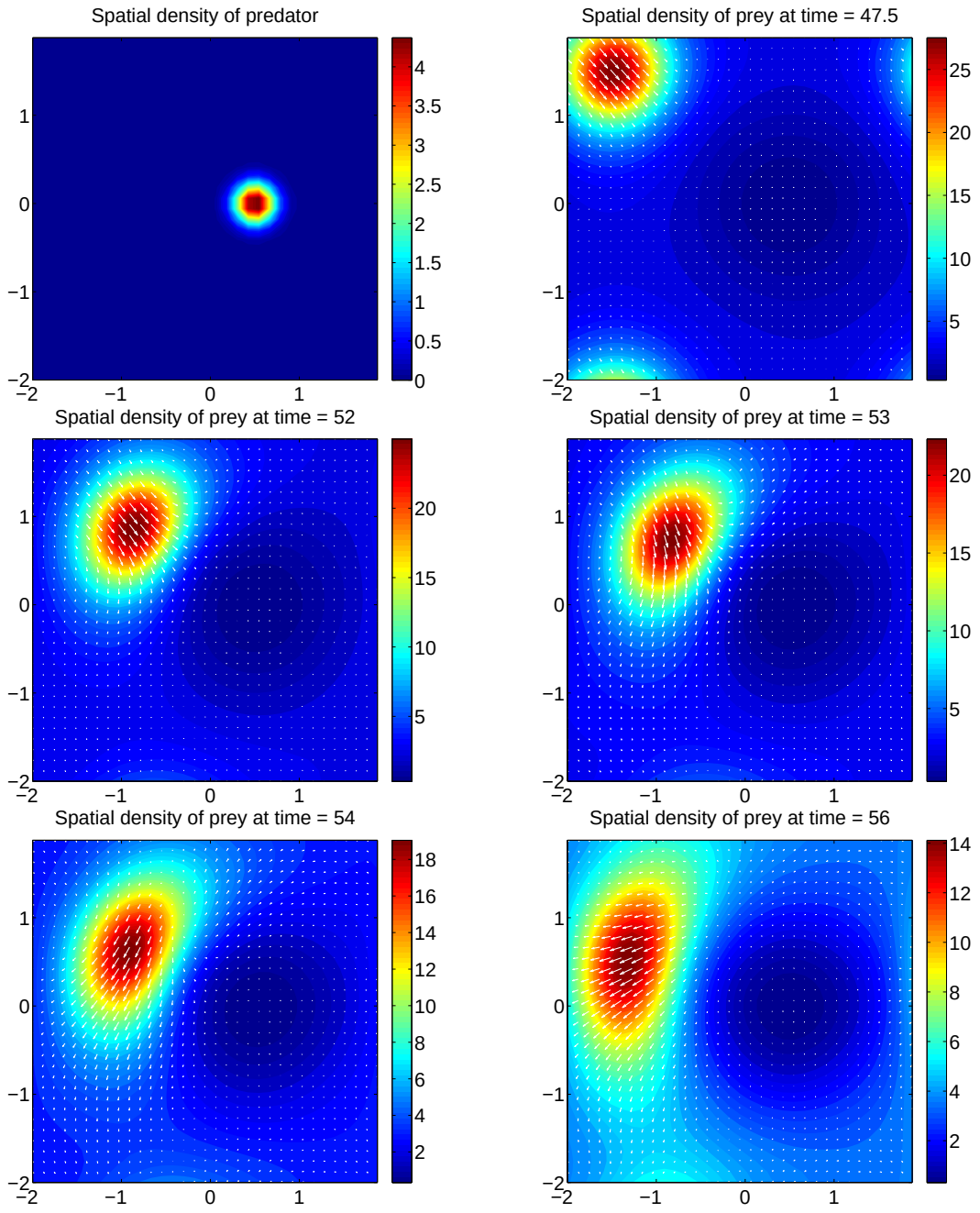

Figure 4.8: Prey avoiding a predator: The prey turn to avoid the predator. The stationary predator is shown in the top left plot. The other five plots show the prey moving towards the predator and the subsequent turning of the prey to avoid the predator. The intensity of the turning is easier to notice when focusing on the change in direction of the white arrows.

Figure 4.9: Bait ball: Dolphins accompanied by a shark force the school of fish into a bait ball. The image is from http://www.nationalgeographic.com.

Dolphins execute herding passes to confine the prey into bait balls [33]. Confining fish in this way makes it more efficient for the dolphins to capture them. The minke whales use either traditional, active entrapment methods or they take advantage of work done by bird rafts, to condense sandeels into a bait ball [27]. A bird raft is a congregation of birds on the surface of the water that has fish underneath on which the birds are feasting. The increase of pressure on the fish allows the minke whales to capture these fish with a minimal amount of effort.

4.3 Moving predator

Even though it is important that the prey behaves realistically around a stationary predator, much more happens when the predator is in motion. A moving predator can cause the prey to turn as a group, to split or to disperse. Since the predator can now come up behind the prey, the prey's blind zone plays a large role in how the group behaves. Also, this section is used as a building block for when the predator is also allowed to turn (see Section 4.4).

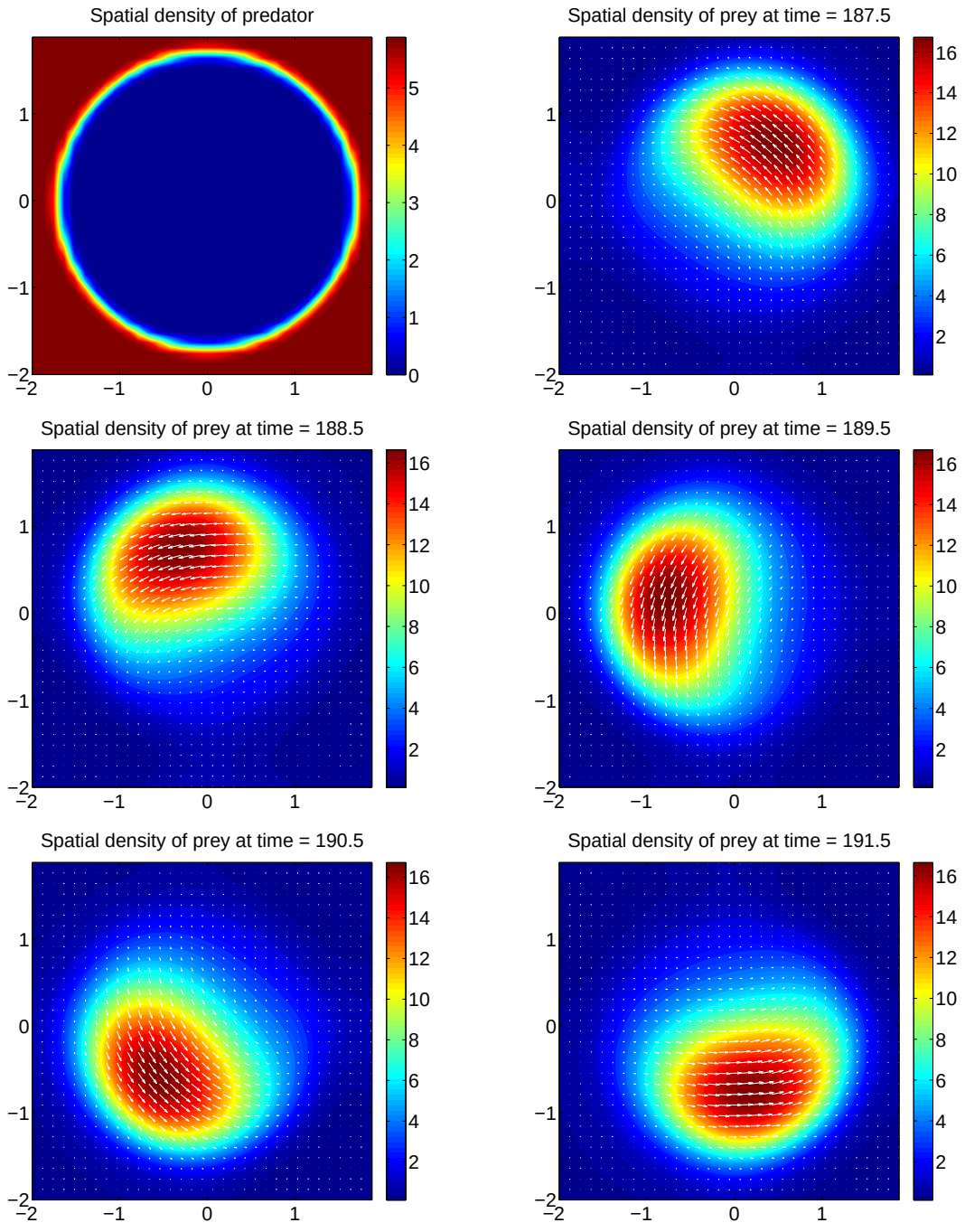

Figure 4.10: Predator ring: A sequence showing the prey enclosed by a predator ring. The top left plot is the predator and the other five are the prey. The prey moves in a circle, continually trying to avoid the predator, but the prey are trapped.

4.3.1 Prey moving towards the predator

In this experiment the initial condition is setup for the prey and predator to collide head on. To simplify the experiment, the predator is a Gaussian bump that moves to the left as time progresses. This means the predator will not change its direction or shape. As the predator moves towards a group of prey, which is also moving towards the predator, the prey behave differently based on the two parameters q_a and q_{al}. The other parameters for this experiment are $q_r = 1$, $q_{rh} = 40$, $k_r = -0.34$ to -0.14, $k_{al} = 0.8$, $k_a = 0.8$ and $k_{rh} = -0.95$. Figure 4.11 shows this experiment, with the plots occurring sequentially from left to right. The top row is the predator. The second row has $q_a = 1$ and $q_{al} = 1$ and shows a splitting of the group. The third row is a different simulation and has $q_a = 1$ and $q_{al} = 5$ and shows a more biased splitting of the group. Since alignment is larger the prey will decide to turn the same way as the majority even if that puts them in harms reach of the predator. The last row is also a different simulation having $q_a = 5$ and $q_{al} = 1$ and shows the group turning around and staying together. Since the attraction is large the prey tries resists splitting and completely turns around to avoid the predator. Eventually the prey will fan out slowly from the constant pursuit of the predator, which is shown in Figure 4.12. This experiment shows a variety of behaviours the model can produce for slight changes in parameters.

This experiment mimics a lunging predator from which the prey must escape by performing an evasive tactic. One tactic is to spread radially outwards from the predator as soon as possible, as seen in [3].

4.3.2 Away from predator - blind zone - alignment

This experiment is designed to see how the blind zone factor affects the behaviour of the prey. Depending on how large the blind zone is, the prey will have more or less information to make a decision to turn to avoid the chasing predator. In Figure 4.13, the top row is the predator and all other plots are the prey. The plots occur sequentially from left to right. The parameters for this experiment are $q_r = 1$, $q_{al} = 5$, $q_a = 1$, $q_{rh} = 40$, $k_r = -0.4$ to -0.3, $k_{al} = 0.8$, $k_a = 0.8$ and $k_{rh} = -0.95$. The second row has $b = -2\pi$ and shows a biased splitting of the group. The value of b being a negative was needed to insure there was no contribution from the blind zone factor. For example, if $b = 0$, there would be a very small blind zone behind the individual. This is a problem from the design of the blind zone kernel, however setting $b = -2\pi$ does not cause any side effects.

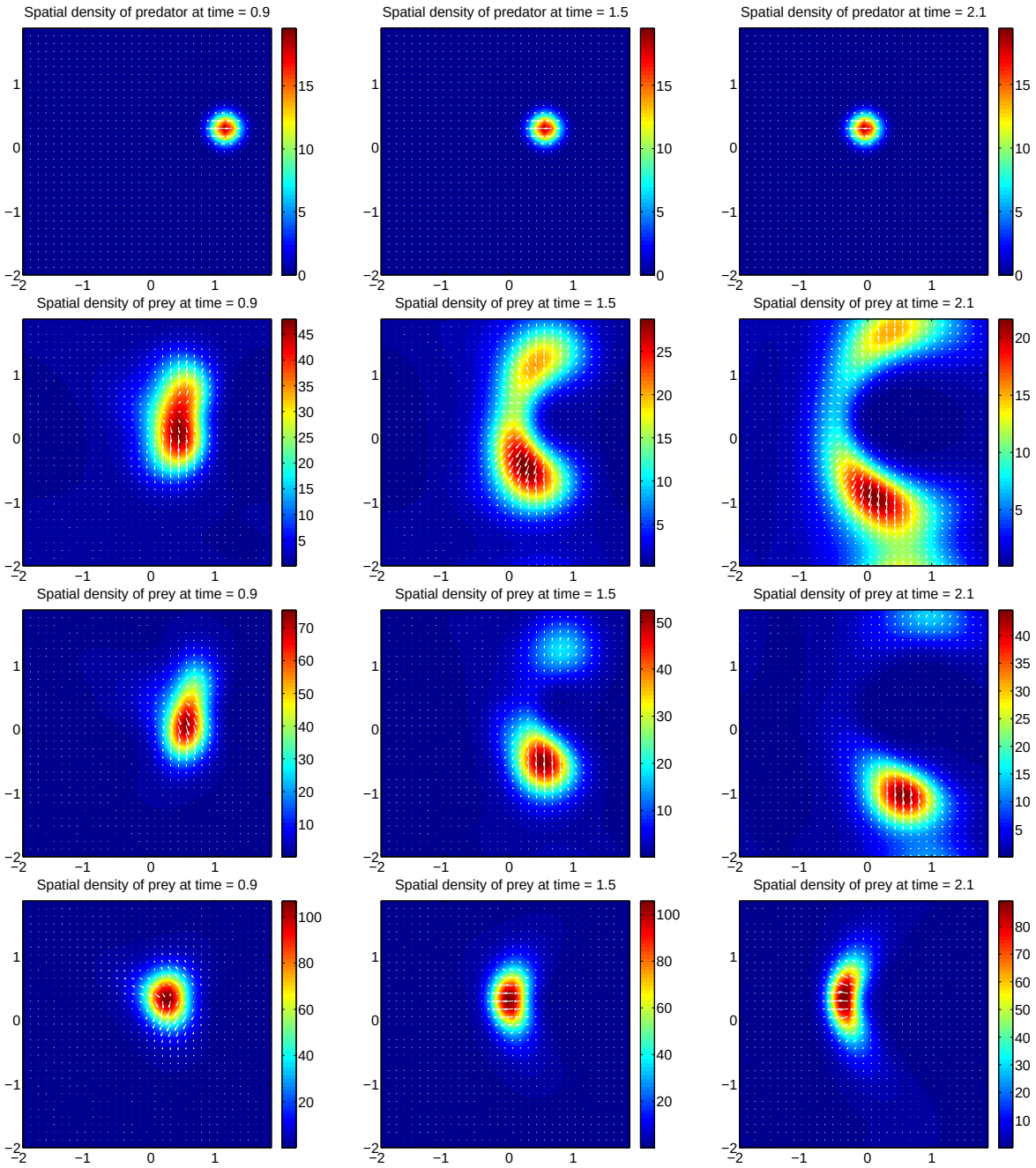

Figure 4.11: Prey moving towards the predator part 1: The plots occur from left to right. The top row is the predator. The second row has $q_a = 1$ and $q_{al} = 1$ and shows the group splitting. A more biased splitting of the group occurs in the third row which has $q_a = 1$ and $q_{al} = 5$. The last row has $q_a = 5$ and $q_{al} = 1$ and shows the group turning completely around, but the group will split as seen in Figure 4.12.

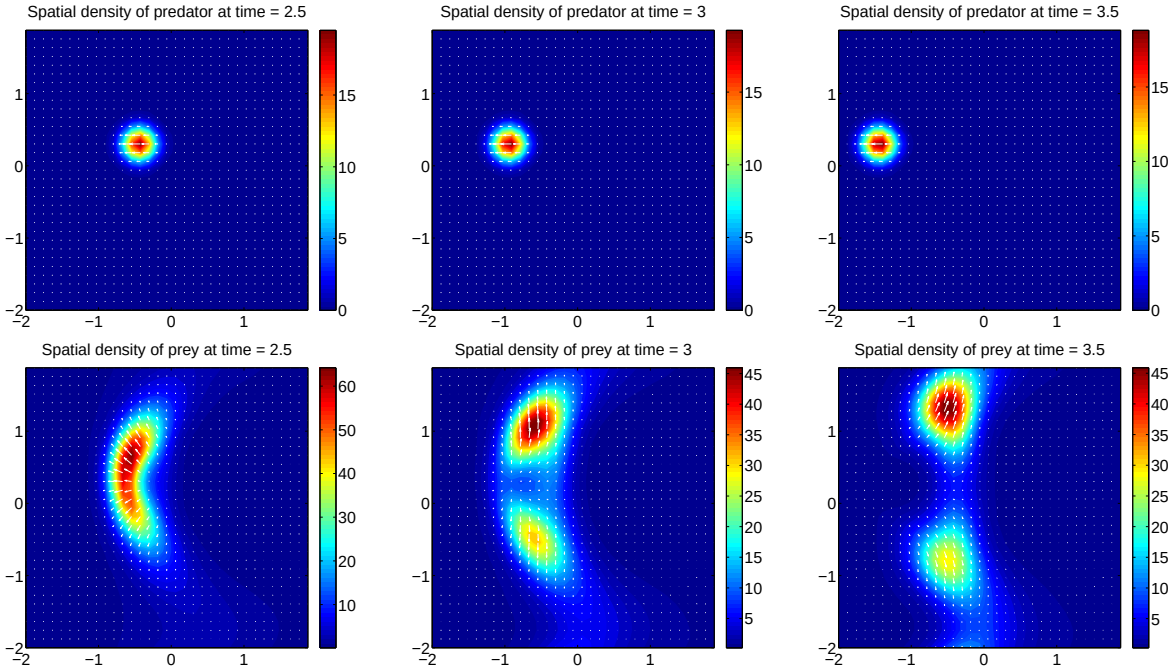

Figure 4.12: Prey moving towards the predator part 2: This is a continuation of the simulation shown in the last row in Figure 4.11. The plots occur sequentially from left to right. The top row is the predator. The bottom row has $q_a = 5$ and $q_{al} = 1$ and shows the group splitting.

The third row has $b = \pi/2$ and shows a less biased splitting of the group. There are slightly more individuals moving down compared to the $b = -2\pi$ case. The last row has $b = \pi$ and shows an even less biased splitting of the group. The only reason this case did not split perfectly into two even groups is because the initial conditions are not symmetric. Since there is no exact solution to our model, it is more appropriate to set the initial conditions from other simulations. Doing this causes inaccuracies. In this experiment, the initial conditions are taken from the end of another experiment which did not have the prey moving directly to the left. The predator, however, does move directly to the left. This slight difference in direction is enough to split the group unevenly. Also, the alignment factor will exaggerate the splitting by bringing more individuals from the smaller group to the larger group.

The increase of the blind zone causes behaviour that can be interpreted as disorientation and confusion among the prey. Another test of the effects of the blind zone was done in [23], where a milling group turned into a carousel group and then into a freely moving group by increasing the blind zone. A carousel group has moving aligned individuals in the outer regions, while the inner regions are unaligned. In a freely moving group, the individuals are not aligned.

4.3.3 Away from predator - blind zone - attraction

This experiment is another example of how the blind zone plays a role in the behaviour of the prey. The parameters and initial conditions are identical to the ones in Section 4.3.2 with the exception of q_a and q_{al}. In Section 4.3.2, $q_a = 1$ and $q_{al} = 5$, while in this experiment $q_a = 5$ and $q_{al} = 1$.

The plots in Figure 4.14 occur sequentially from left to right. The top row is the predator. The second row has $b = -2\pi$ and shows a high density group turning together to avoid the predator. As discussed earlier, $b = -2\pi$ is equivalent to no blind zone. The third row has $b = \pi/2$ and shows a greater amount of turning. The last row has $b = \pi$, and shows less density and a slight separation of individuals from the group. When the prey have a blind zone of π, there is not a lot of information transferred between the individuals, which can cause confusion. Since $q_a = 5$ one would think the group would stay together, but because of the blind zone this does not happen.

More interesting than the $b = \pi$ case is the $b = \frac{\pi}{2}$ case. Looking at the small arrows inside the spatial density of the prey at time 0.48 for the $b = \frac{\pi}{2}$ case, one can see that the individuals are moving up to the right. In the other two cases, the individuals are moving up and slightly to the

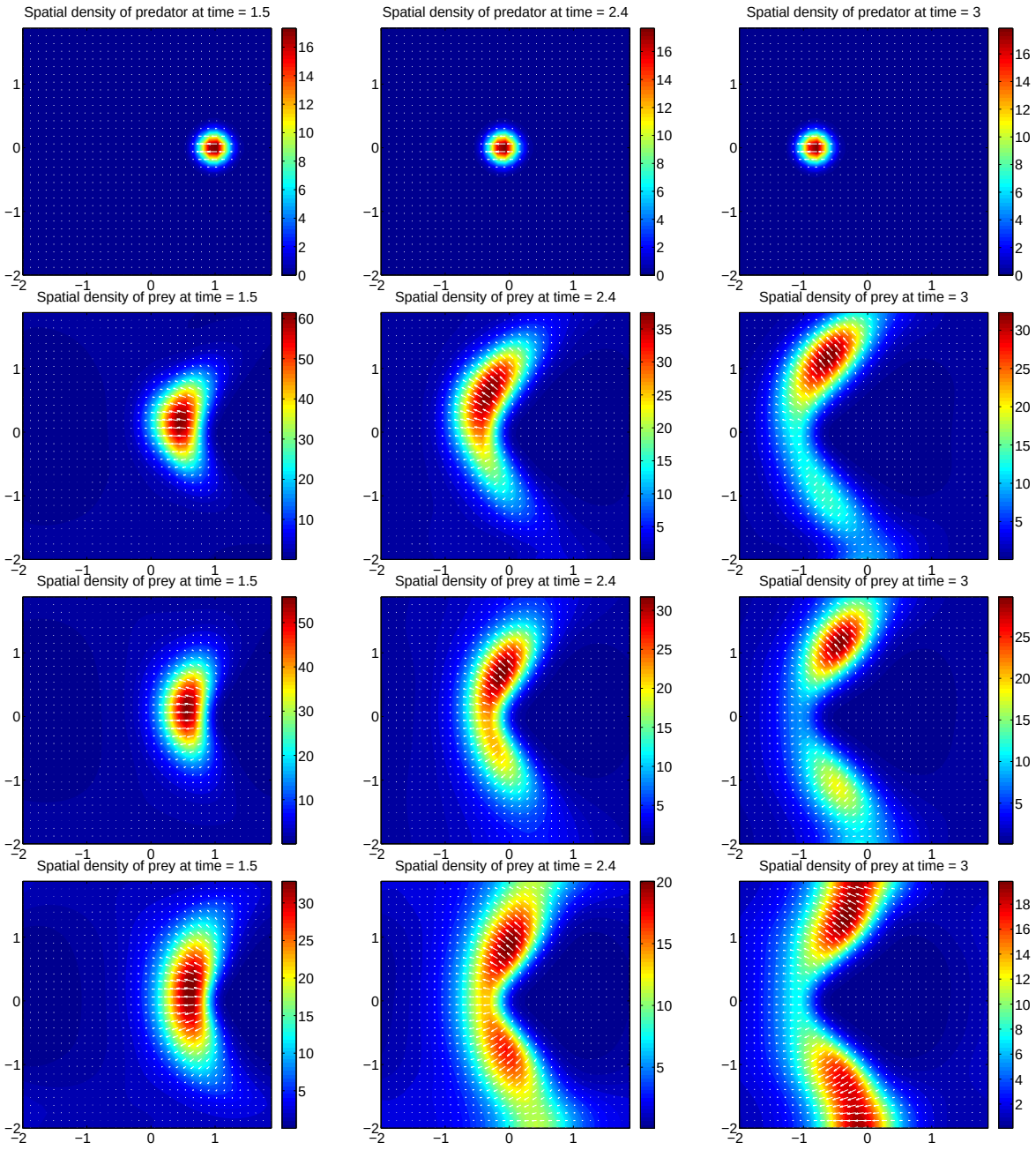

Figure 4.13: Away from predator - blind zone - alignment: The predator is set to chase the prey from inside the prey's blind zone. The plots occur sequentially from left to right. The top row is the predator, while the next three rows are the prey with the blind zone width b equal to -2π (zero blind zone), $\frac{\pi}{2}$ and π, respectively. The prey's main concerns are to avoid the predator and to align with the group due to the large value of q_{al}.

left. Some fish will swim in a circle and arrive back at their starting point when a lunging predator comes by [3,29]. This behaviour was not captured, due to complications with the periodic boundary conditions, but the case with $b = \frac{\pi}{2}$ shows some promise that this behaviour can be captured. One can imagine that if the predator is to continue moving to the left, if the boundary conditions are nonexistent and if there are two groups that avoided the predator, then these two groups would then be attracted together and eventually reform the original group.

The tight turning behaviour shown in Figure 4.14 is seen in the prey species of the Eleonora's falcon [18]. One tactic prey can use to avoid a predator is to initiate tight turns at high speed. Since the Eleonora's falcon is larger than its prey, the prey have a higher chance of escape when using this tactic.

4.4 Turning predator

While a predetermined behaviour of a predator can capture small moments of believable reactions in prey, a turning predator is much more realistic. The predator can now react to its surroundings. Equations (2.43), (2.48) and (2.49) are now implemented for all remaining experiments to describe the predator. Since the predator is no longer a fixed shape, it is better to think of the predator as a group of predators.

4.4.1 Splitting of the prey

In this experiment the predators chase the prey and successfully splits them apart (see Figure 4.15). The initial condition for this simulation is a random distribution in space and angle. The parameters for this experiment are $q_r = 1.1725$, $q_{al} = 3.8003$, $q_a = 3.8983$, $q_{rh} = 49.8711$, $\bar{q}_r = 7.3279$, $\bar{q}_a = 10.6207$, $\bar{q}_{ap} = 24.0813$, $k_r = -0.0954$, $k_{al} = 0.6036$, $k_a = 0.6490$, $k_{rh} = -0.99$, $\bar{k}_r = -0.5$, $\bar{k}_a = 0.8$ and $\bar{k}_{ap} = 0.95$. The parameters favour the attraction and alignment effects of the prey, but when the predators get too close the repulsion from the predators on the prey are too great for the group to stay together. As this happens some of the prey will want to move away from the group, ignoring any group cohesiveness. This can cause confusion in the prey and the group could fan out or split into two separate groups, which will make it easier for the predators to catch the prey. This is a classic case of predators running into a group of prey.

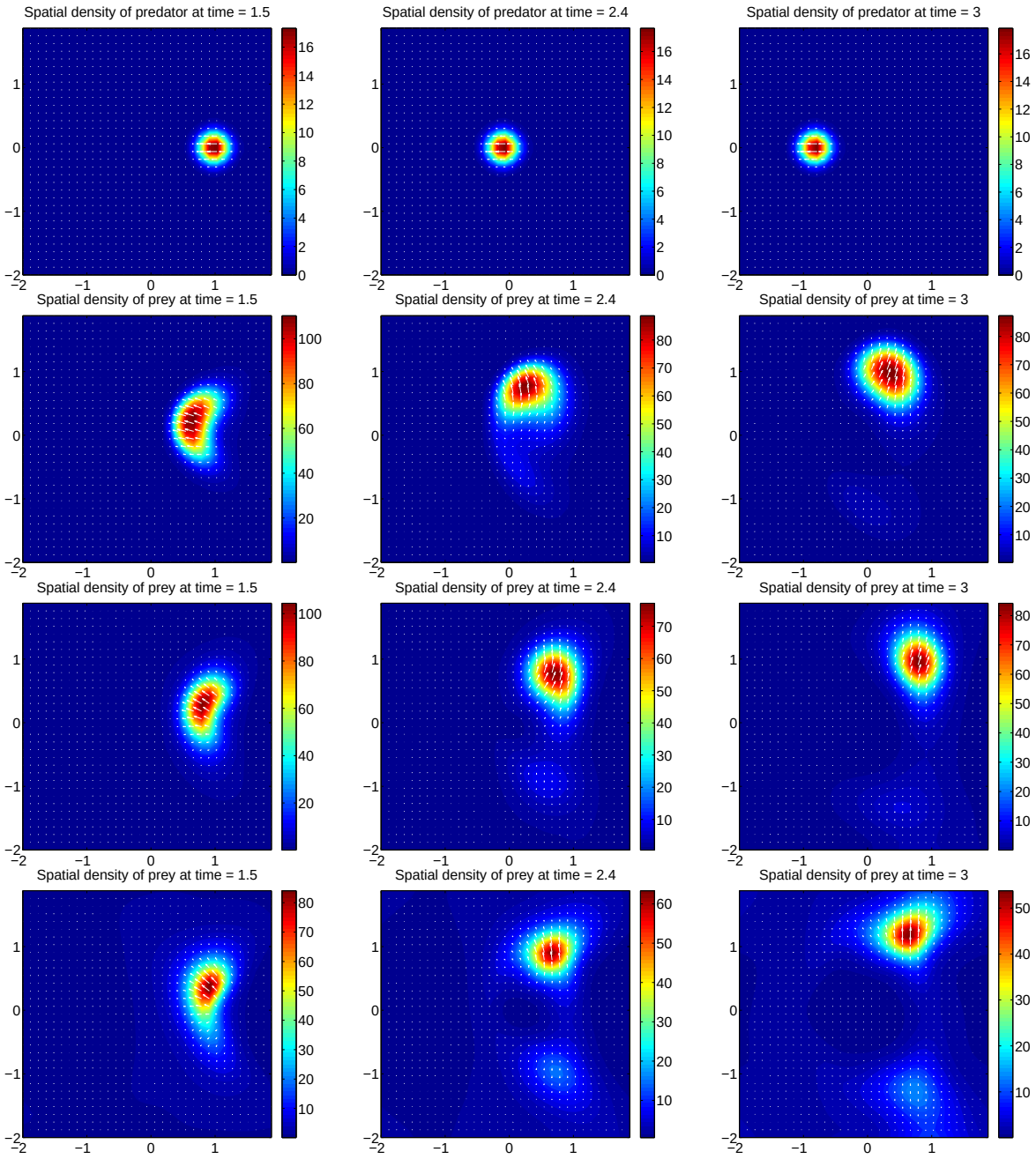

Figure 4.14: Away from predator - blind zone - attraction: The predator is set to chase the prey from inside the prey's blind zone. The plots occur sequentially from left to right. The top row is the predator, while the next three rows are the prey with the blind zone width b equal to -2π (zero blind zone), $\frac{\pi}{2}$ and π, respectively. The prey's main concerns are to avoid the predator and to stay together due to the large value of q_a.

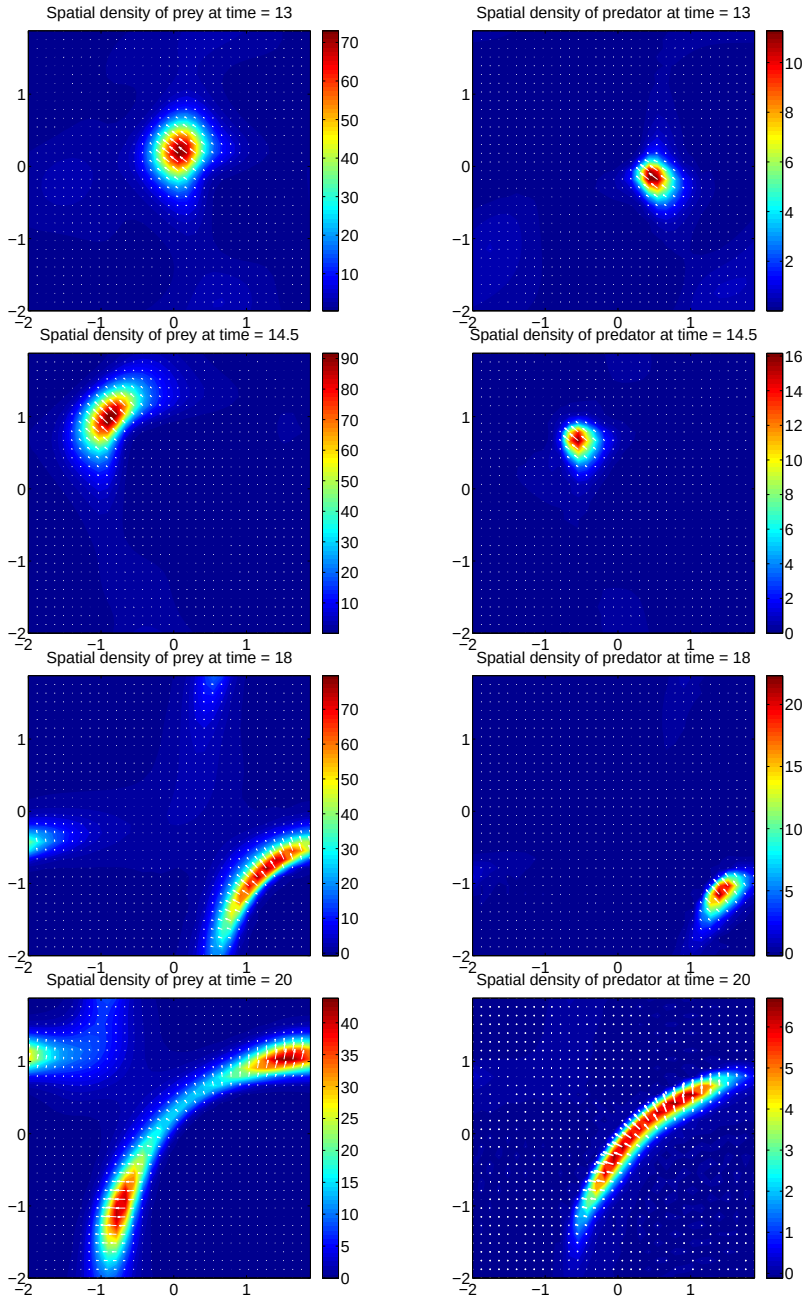

Figure 4.15: Splitting of the prey: The prey are shown in the left column while the predators are shown in the right. As the predators pursue the prey, the prey splits apart.

4.4.2 Dispersal of the prey

In this experiment the prey disperse from the group in order to save themselves (see Figure 4.16). This is a common dispersing behaviour called "flash expansion", discussed in [3, 26], where the prey only focus on making the distance between themselves and the predators larger. Because the predators follow the largest density, the individuals that break off from the group have a higher likelihood of escaping. In order to notice the dispersal of the prey in Figure 4.16, it is important to pay attention to the change in the magnitude of the population densities. The initial condition for this experiment is at time step 2.9 of the simulation from Section 4.4.1, which has been shifted for better visualization. The parameters that are used in this experiment are $q_r = 2$, $q_{al} = 5$, $q_a = 5$, $q_{rh} = 8$, $\bar{q}_r = 8$, $\bar{q}_a = 16$, $\bar{q}_{ap} = 6$, $k_r = -0.6$, $k_{al} = 0.6$,$k_a = 0.6$, $k_{rh} = -0.95$, $\bar{k}_r = -0.6$, $\bar{k}_a = 0.6$ and $\bar{k}_{ap} = 0.95$. Also, the blind zone width is not the same as other experiments ($b \neq \frac{\pi}{2}, b = 3.6652$). The change of the blind zone width can cause more confusion among the prey. Once the prey scatter, they travel away from the group and cannot get any information from behind them, therefore they have no impetus to regroup.

4.4.3 Slow predators

In this experiment the predators' speed has been reduced from $\gamma_h = 1$ to $\gamma_h = 0.25$. At this speed the predators have a difficult time catching prey. The group that depicts the predators stays in a similar spot throughout the simulation with only subtle movements when the prey get close, as seen in Figure 4.17. Once the prey are out of range, the predators have no incentive to move, therefore they stay in one spot. Since the predators have no alignment, they will not move in unison and each individual will turn into the centre of the group. Figure 4.17 shows three progressive steps in time for the prey in the left column and the predators in the right column. The prey move up to the left towards the predators and then is deflected to the left. The predators try to reach for the prey but the prey are gone too quickly. The parameters for this experiment are $q_r = 2$, $q_{al} = 5$, $q_a = 5$, $q_{rh} = 8$, $\bar{q}_r = 8$, $\bar{q}_a = 16$, $\bar{q}_{ap} = 6$, $k_r = -0.6$, $k_{al} = 0.6$, $k_a = 0.6$, $k_{rh} = -0.95$, $\bar{k}_r = -0.6$, $\bar{k}_a = 0.6$ and $\bar{k}_{ap} = 0.95$. The reason q_{rh} is lower for this experiment compared to other experiments is because we wanted the prey to get close to the predator before it turns away.

A slow predator is at a huge disadvantage when trying to capture prey. In nature, predators are not usually 75% slower than the prey, as in Figure 4.17. A predator with this sort of speed must

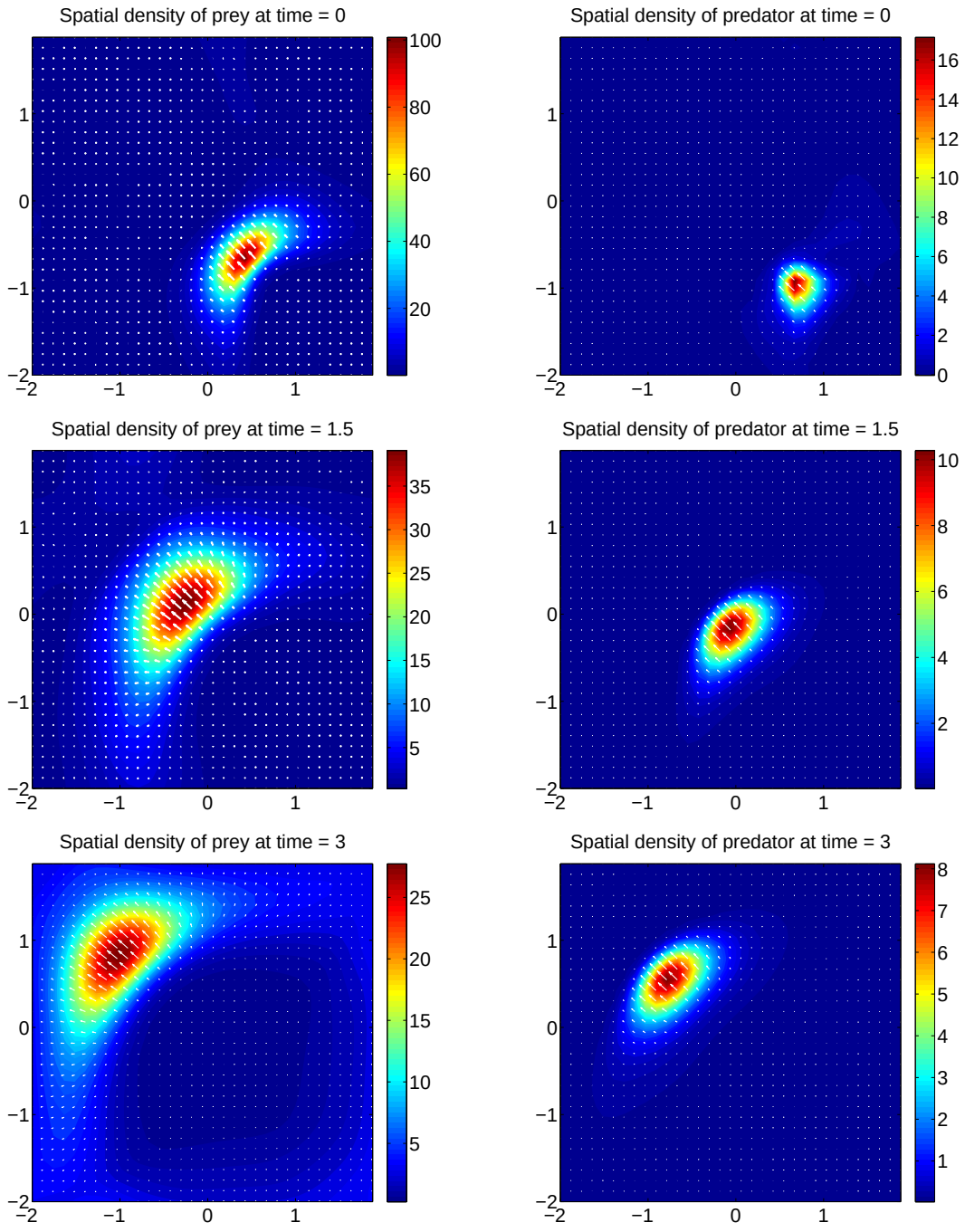

Figure 4.16: Dispersal of the prey: The prey are shown in the left column, while the predators are shown in the right column. The plots show a sequence of the predators dispersing the prey. Note the decrease in magnitude of the population densities, particularly of the prey.

evolve quickly or think of another method to capture its prey otherwise it will not survive. Frogfish, which are slow predators, have a very fast capture technique. They wait for their prey to get close and they use an enormous suction pressure to engulf their prey [15].

4.4.4 Fast predators

In this experiment the predators' speed is increased from $\gamma_h = 1.0$ to $\gamma_h = 1.5$. The predator can now move faster than the prey. A steady state is reached where the predators occupy the same location as the prey and they both move in the same direction with the same speed. The predators are exploiting the slowness of the prey and this it can be thought of as the predators feasting on the prey (see Figure 4.18). The initial condition for this experiment is the time step 2.9 of the simulation from Section 4.4.1. The parameters for this experiment are the same as the slow predators experiment in Section 4.4.3, with the exception of γ_h. The plots on the left of Figure 4.18 show the prey, while the right plots show the predators. This shows how the prey and predators move up to the left and do not change form. A translational steady state is thereby achieved.

In nature, predators are often not 50% faster than the prey. In this case the predator would eat all of the prey and the prey would not have a chance to evolve to be faster. However, this speed discrepancy is common when fish are in their juvenile stages. Often slow individuals will find places to hide or use other defences. Moving quickly for a predator is a huge advantage for a predator to capture prey. The tuna and the lamnid shark have evolved to have counter-current heat-exchange mechanisms for conserving metabolic heat and raising their body temperatures [6]. Warmer muscles give extra power and create faster swimming.

4.4.5 Double predator split

This experiment shows how the predators can be clever about how they catch prey. The initial condition is a random distribution is space and angle. The parameters for this experiment are $q_r = 1.8676$, $q_{al} = 4.3989$, $q_a = 5.9724$, $q_{rh} = 50$, $\bar{q}_r = 8$, $\bar{q}_a = 10$, $\bar{q}_{ap} = 24$, $k_r = -0.6$, $k_{al} = 0.6$, $k_a = 0.6$, $k_{rh} = -0.95$, $\bar{k}_r = -0.5$, $\bar{k}_a = 0.8$, $\bar{k}_{ap} = 0.95$ and $\gamma_h = 2$. These parameters are in perfect balance, making both the predator and prey stay in groups but also allowing them to split quickly if they need to. Figure 4.19 shows a sequence of two groups of predators working together to split the prey. The left column is the prey while the right column are the predators. The top

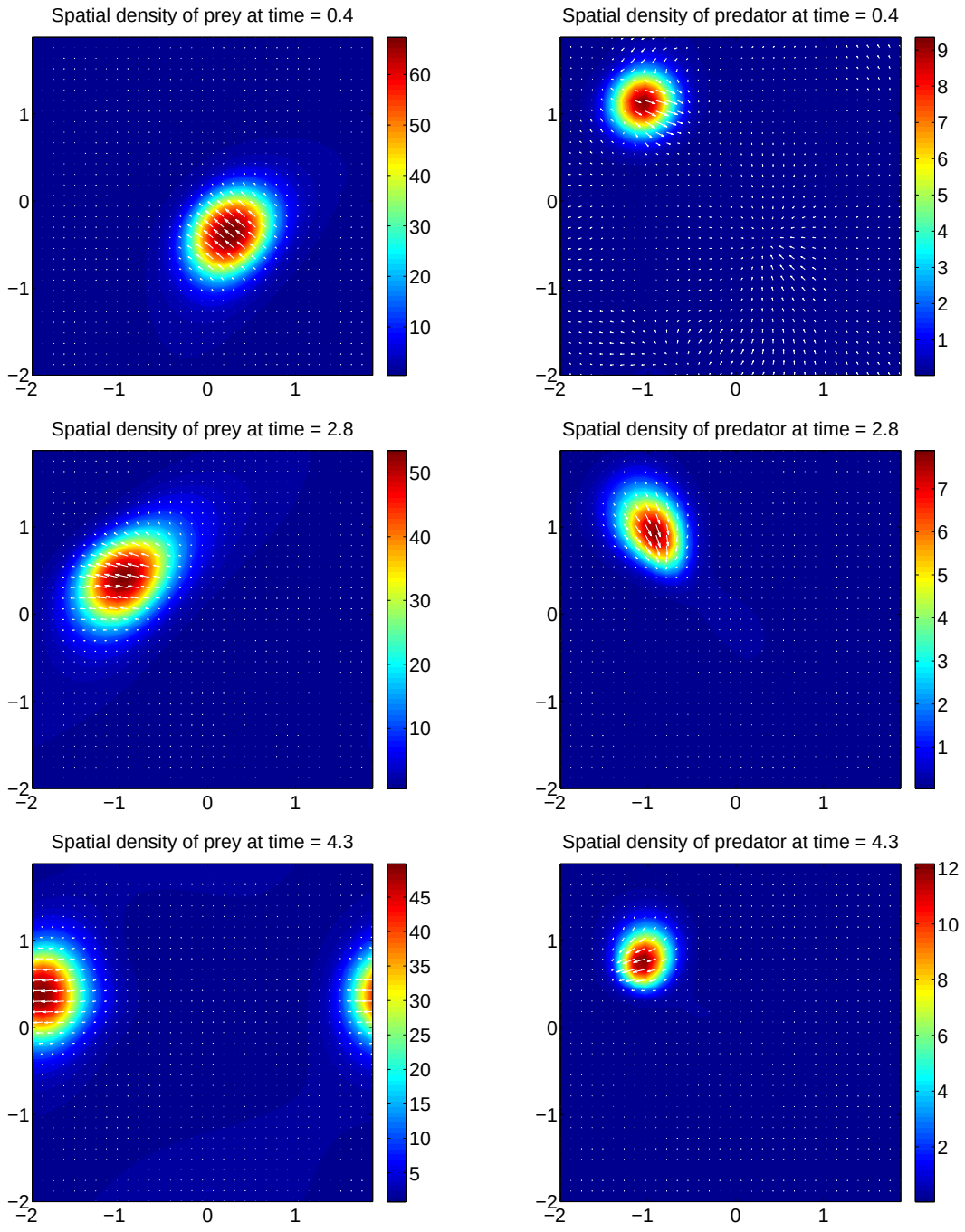

Figure 4.17: Slow predators: The prey are shown in the left column, while the predators are shown in the right column. Slow predators, $\gamma_h = 0.25$, cannot catch their prey. The predators make an attempt when the prey come close but are unsuccessful.

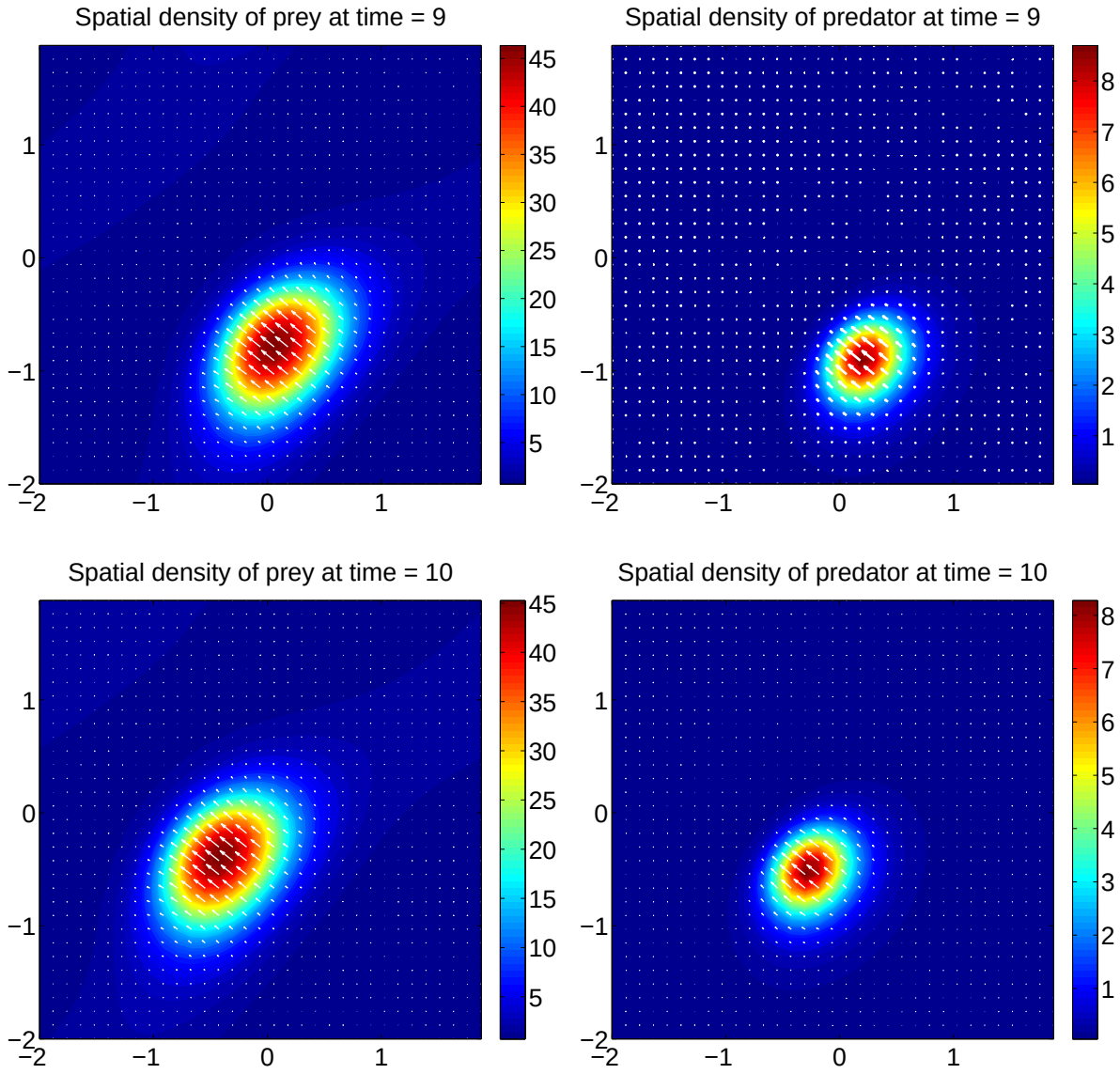

Figure 4.18: Fast predators: The prey are shown in the left column, while the predators are shown in the right column. Fast predators, $\gamma_h = 1.5$, can catch up and keep up with their prey. This translational steady state shows the predators feasting.

row shows the predators splitting to follow the two separate groups of prey. The middle two plots show the two predator groups trapping the prey. The bottom row shows the prey escaping from both predator groups by moving up or down as the predators collide. After the prey split up and down, they merge again and then split left and right, which brings them back to the first plot again in Figure 4.19. This is a recurring pattern and there are likely many more to find with this model.

Wild dogs show elaborate hunting techniques (see Figure 4.20). They have one of the highest capture rates of any predator on the savanna [17]. Their techniques favour stamina instead of speed, and their ability to work as a group. In order to tire out and capture the prey, the group members take turns chasing the prey while trailing dogs conserve their stamina. Eventually the slow prey, such as young, old or sick individuals, will get tired and be caught [17]. The ability of predators to split and work as a team is showcased in Figure 4.19. Though all of the complexities of the wild dog's hunting techniques are not captured here, this model has captured a team effort by predators.

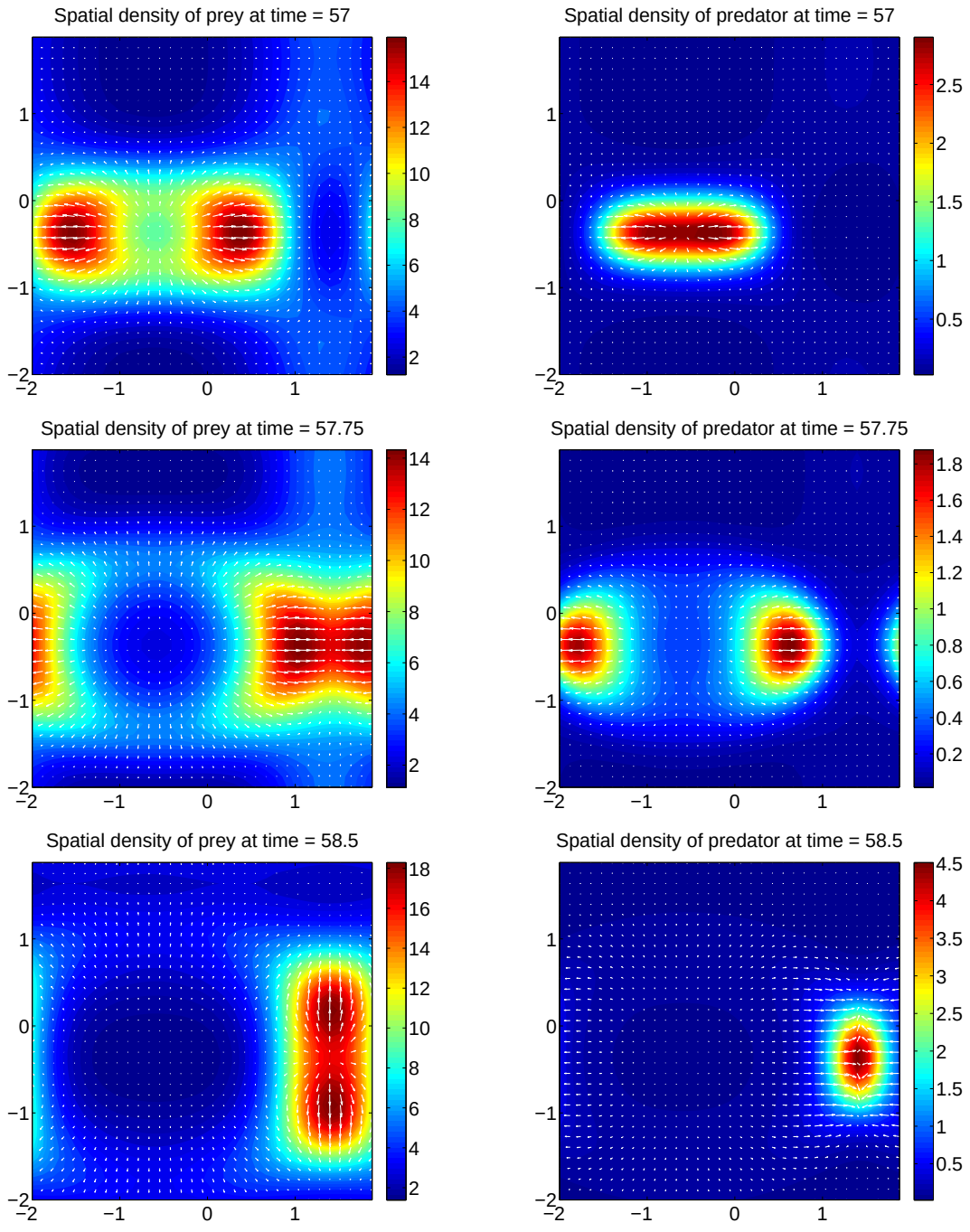

Figure 4.19: Double predator split: The prey are shown in the left column, while the predators are shown in the right column. The predators work as a team when chasing the prey. The predators come towards the group of prey from two angles and force the prey to split.

Figure 4.20: Wild dogs: A Wildebeest is being chased by a pack of wild dogs. The image is from http://www.arkive.org

Chapter 5

Conclusion

We have extended the two dimensional nonlocal kinetic model proposed in [13] to include a blind zone and a predator. The predator's sophistication was increased in stages: no predator, stationary predator, a moving predator that does not sense its surroundings and a moving predator that reacts to its surroundings. For each progression of the predator, simulations were done to showcase the accuracy of the model. The behaviours obtained for the no predator are: oval swarm, collision of two groups, cluster size and milling. The behaviours obtained for the stationary predator are: prey near a predator and food, prey avoiding a predator, and predator ring. The behaviours obtained for the moving predator that does not sense its surroundings are: prey moving towards the predator, away from predator - blind zone - alignment, and away from predator - blind zone - attraction. The behaviours obtained for the moving predator that reacts to its surroundings are: splitting of the prey, dispersal of the prey, slow predators, fast predators, and double predator split.

The predator, in its final version, is formulated with the same equations as the prey, making the model cohesive. Both prey and predator are influenced by repulsion and attraction with themselves. The prey is repelled by the predator, while the predator is attracted to the prey. The prey can align with other members inside its group, however the predator does not have this ability. This model in the future should incorporate the alignment of the predator. This will allow the predator to be thought of as a group instead of a solitary predator.

One can replicate the process of incorporating a predator to any desired number of predators or prey. For example, we could add a second predator that competes with the first predator for the prey.

Therefore the model can be extended to include any combination of species. With an addition of a predator, we could incorporate predator intelligence into future work. This could have the predators using group techniques to capture the prey even though the predator may not be able to catch the prey by themselves.

With the addition of the blind zone and the predator, the number of parameters in the model has roughly doubled. With a very large parameter space, it is difficult to know what parameters produce certain interesting behaviours. A large parameter search could be run on multiple computers for many months to get a better understanding of how the parameters affect the aggregate behaviour of animals in the model.

Bibliography

[1] T. Balch and R. C. Arkin, *Behavior-based formation control for multi-robot teams*, IEEE Transactions on Robotics and Automation **14** (1998), no. 6, 926–939.

[2] E. Barbera, C. Curró, and G. Valentia, *Wave features of a hyperbolic prey-predator model*, Math. Meth. Appl. Sci. **33** (2010), 1504–1515.

[3] S. Camazine, J.-L. Deneubourg, N. R. Franks, J. Sneyd, G. Theraulaz, and E. Bonabeau, *Self-organization in biological systems*, Princeton Studies in Complexity, Princeton University Press, Princeton, NJ, 2001.

[4] R. S. Cantrell and C. Cosner, *Models for predator-prey systems at multiple scales*, SIAM J. Appl. Math. **38** (1996), no. 2, 256–286.

[5] C. Canuto, M. Y. Hussaini, A. Quarteroni, and T. A. Zang, *Spectral methods in fluid dynamics*, Springer Series in Computational Physics, Springer-Verlag, New York, 1988.

[6] G. Carey, J. M. Teal, J. W. Kanwisher, K. D. Lawson, and J. S. Beckett, *Warm-bodied fish*, American Zoologist **11** (1971), 135–143.

[7] C. Cercignani, R. Illner, and M. Pulvirenti, *The mathematical theory of dilute gases*, Applied Mathematical Sciences, vol. 106, Springer-Verlag, New York, 1994.

[8] D. J. Cook, P. Gmytrasiewicz, and L. B. Holder, *Decision-theoretic cooperative sensor planning*, IEEE Transactions on Pattern Analysis and Machine Intelligence **18** (1996), no. 10, 1013–1023.

[9] I. D. Couzin, J. Krause, R. James, G.D. Ruxton, and N. R. Franks, *Collective memory and spatial sorting in animal groups*, J. Theor. Biol. **218** (2002), 1–11.

[10] L. Edelstein-Keshet and B. Ermentrout, *Models for contact-mediated pattern formation: cells that form parallel arrays*, J. Math. Biol. **29** (1990), 33–58.

[11] R. Eftimie, G. de Vries, and M. A. Lewis, *Complex spatial group patterns result from different animal communication mechanisms*, Proc. Natl. Acad. Sci. **104** (2007), no. 17, 6974–6979.

[12] R. Eftimie, G. de Vries, M. A. Lewis, and F. Lutscher, *Modeling group formation and activity patterns in self-organizing collectives of individuals*, Bull. Math. Biol. **69** (2007), no. 5, 1537–1566.

[13] R.C. Fetecau, *Collective behavior of biological aggregations in two dimensions: A nonlocal kinetic model*, Mathematical Models and Methods in Applied Sciences **21** (2011), no. 7, 1539–1569.

[14] E. Geigant, K. Ladizhansky, and A. Mogilner, *An integrodifferential model for orientational distributions of F-actin in cells*, SIAM J. Appl. Math. **59** (1998), no. 3, 787–809.

[15] D. B. Grobecker and T. W. Pietsch, *High-speed cinematographic evidence for ultrafast feeding in antennariid anglerfishes*, Am. Ass. Adv. Sci. **205** (1979), no. 4411, 1161–1162.

[16] N. O. Handegard, K. M. Boswell, C. C. Ioannou, S. P. Leblanc, D. B. Tjøstheim, and I. D. Couzin, *The dynamics of coordinated group hunting and collective information transfer among schooling prey*, Current Biology **22** (2012), 1–5.

[17] M. W. Hayward, J. O'Brien, M. Hofmeyr, and G. I. H. Kerley, *Prey preferences of the african wild dog lycaon pictus (canidae: Carnivora): Ecological requirements for conservation*, J. Mammalogy **87** (2006), 1122–1131.

[18] A. Hedenström and M. Rosén, *Predator versus prey: on aerial hunting and escape strategies in birds*, Int. Soc. Behav. Ecology **12** (2001), no. 2, 150–156.

[19] W. Liu, C. Fu, and B. Chen, *Hopf bifurcation and center stability for a predator - prey biological economic model with prey harvesting*, Comm. Nonlin. Sci. Num. Sim. **17** (2012), no. 10, 3989–3998.

[20] R. Lukeman, Y.-X. Li, and L. Edelstein-Keshet, *A conceptual model for milling formations in biological aggregates*, Bull. Math. Biol. **71** (2009), no. 2, 352–382.

[21] A. Mogilner and L. Edelstein-Keshet, *A non-local model for a swarm*, J. Math. Biol. **38** (1999), 534–570.

[22] W. W. Murdoch, *Switching in general predators: Experiments on predator specificity and stability of prey*, Ecological Monographs **39** (1969), no. 4.

[23] J. P. Newman and H. Sayama, *Effect of sensory blind zones on milling behavior in a dynamic self-propelled particle model*, Phys. Rev. E **78** (2008), no. 011913.

[24] J. K. Parrish, *Using behavior and ecology to exploit schooling fishes*, Environ. Biol. Fish. **55** (1999), 157–181.

[25] J. K. Parrish and L. E. Keshet, *Complexity, pattern, and evolutionary trade-offs in animal aggregation*, Science **284** (1999), 99–101.

[26] T. J. Pitcher and J. K. Parrish, *Functions of shoaling behaviour in teleosts*, Chapman & Hall, 1993.

[27] K. P. Robinson and M. J. Tetley, *Behavioural observations of foraging minke whales (balaenoptera acutorostrata) in the outer moray firth, north-east scotland*, J. Mar. Biol Ass. U.K. **87** (2007), 85–86.

[28] R. A. Rountree and G. R. Sedberry, *A theoretical model of shoaling behavior based on a consideration of patterns of overlap among the visual fields of individual members*, J. Acta Ethol. **12** (2009), 61–70.

[29] D. J. T. Sumpter, *Collective animal behavior*, Princeton University Press, Princeton, N.J., 2010.

[30] C. M. Topaz and A. L. Bertozzi, *Swarming patterns in a two-dimensional kinematic model for biological groups*, SIAM J. Appl. Math. **65** (2004), 152–174.

[31] C. M. Topaz, A. L. Bertozzi, and M. A. Lewis, *A nonlocal continuum model for biological aggregation*, Bull. Math. Bio. **68** (2006), 1601–1623.

[32] R. Vabø and L. Nøttestad, *An individual based model of fish school reactions: predicting antipredator behaviour as observed in nature*, Fish. Oceanogr. **117** (1997), 155–171.

[33] R. L. Vaughn, E. Muzi, J.L. Richardson, and B. Würsig, *Dolphin bait-balling behaviors in relation to prey ball escape behaviors*, J. Ethology **117** (2011), 859–871.

[34] K. A. J. White, J. D. Murray, and M. A. Lewis, *Wolf-deer interactions: a mathematical model*, Proc. R.Soc. Lond. B **263** (1996), 299–305.